

Complexities of landscape evolution during incision through layered stratigraphy with contrasts in rock strength

Adam M. Forte,^{1*} Brian J. Yanites² and Kelin X. Whipple¹

¹ School of Earth and Space Exploration, Arizona State University, Tempe, AZ, USA

² Department of Geological Sciences, University of Idaho, Moscow, ID, USA

Received 3 September 2015; Revised 16 March 2016; Accepted 17 March 2016

*Correspondence to: Adam M. Forte, School of Earth and Space Exploration, Arizona State University, 781 E. Terrace Mall, Tempe, AZ 85287-6004, USA. E-mail: aforte@asu.edu



ABSTRACT: Variation in the erodibility of rock units has long been recognized as an important determinant of landscape evolution but has been little studied in landscape evolution models. We use a modified version of the Channel-Hillslope Integrated Landscape Development (CHILD) model, which explicitly allows for variations in rock strength, to reveal and explore the remarkably rich, complex behavior induced by rock erodibility variations in even very simple geologic settings with invariant climate and tectonics. We study the importance of relative contrasts in erodibility between just two units, the order of these units (whether hard rocks overlie soft or soft rocks overlie hard) and the orientation of the contact between the two units. We emphasize the spatial and temporal evolution of erosion rates, which have important implications for basin analysis, detrital mineral records, and the interpretation of cosmogenic isotope concentrations in detrital samples. Results of the landscape evolution modeling indicate that the stratigraphic order of units in terms of erodibility, the gross orientation of the contact (i.e. dipping away or toward the outlet of the landscape) and the contact dip angle all have measurable effects on landscape evolution, including significant spatial and temporal variations in erosion rates. Steady-state denudation conditions are unlikely to develop in landscapes with significant contrasts in rock strength in horizontal to moderately tilted rock layers, at least at the scale of the entire landscape. Additionally, our results demonstrate that there is no general relation between rock erodibility and erosion rates in natural settings. Although rock erodibility directly controls the erosion rate constant in our models, it is not uncommon for higher erosion rates to occur in the harder, less erodible rock. Indeed erosion rates may be either greater or less than the rock uplift rate (invariant in time and space in our models) in both hard and soft rocks, depending on the local geology, topography, and the pattern of landscape evolution. Copyright © 2016 John Wiley & Sons, Ltd.

KEYWORDS: landscape evolution; erodibility; rock strength; detrital mineral records; steady state

Introduction

The topographic form of a landscape represents a competition between (1) uplift of rocks driven by tectonic processes and (2) climatically and lithologically mediated erosion; thus topography encodes a record of the tectonic and climatic history of a region (e.g. Ahnert, 1970; Whipple and Tucker, 1999; Wobus *et al.*, 2006; Kirby and Whipple, 2012; Whittaker, 2012). Often implicit in the interpretation of tectonics or climate from topography is the concept that landscapes tend to reach a steady-state condition where the long-term erosion rate equals the uplift rate and that transience within a landscape, i.e. identified as a migrating boundary that separates two distinct topographic states, conveys information regarding changes in either climate, tectonics, or a combination of the two (e.g. Montgomery, 2001; Whipple, 2001; Willett *et al.*, 2001; Willett and Brandon, 2002; Gasparini *et al.*, 2007). Importantly, the concept that landscapes will reach a steady-state denudational condition is largely predicated on the implicit but rarely stated assumption that the spatial distribution of rock erodibility is stationary. Natural landscapes are typically characterized by significant spatial heterogeneities

in erodibility, driven by variability in the inherent strength of different rock units (e.g. Sklar and Dietrich, 2001; Goode and Wohl, 2010; Lamb *et al.*, 2015), pervasiveness or orientation of fractures (e.g. Miller, 1990; Weissel and Seidl, 1997; Whipple *et al.*, 2000; Hartshorn *et al.*, 2002; Molnar *et al.*, 2007; Lamb and Dietrich, 2009; Lifton *et al.*, 2009; Clarke and Burbank, 2010; Marshall and Roering, 2014); orientation of bedding planes (e.g. Miller, 1990; Oskin *et al.*, 2014), and details of the stratigraphy such as thickness of units or the strength of the weakest rock within a stratigraphic package (e.g. Wohl *et al.*, 1994; Schmidt and Montgomery, 1995; Montgomery, 2004). Contacts between rock units of variable erodibility are rarely vertical. Consequently the spatial distribution of the erodibility of exposed rock units, which is a function of the stratigraphic and tectonic legacy of a given setting, will vary over time. The exhumation and fluvial dissection of disparate rock units has interesting, and surprisingly complex, implications for the pace and style of landscape evolution, spatio-temporal patterns of erosion rate, and the extent to which steady-state conditions are achievable in landscapes characterized by contrasts in rock strength.

The erodibility of rock has been long recognized as an important factor in various aspects of the topographic form of a landscape including the spatial distribution of hillslope gradients, drainage density, longitudinal river profile shape, and total relief (e.g. Gilbert, 1877; Hack, 1960; Schumm and Lichty, 1965; Leopold and Bull, 1979; Miller, 1990; Wohl *et al.*, 1994; Weissel and Seidl, 1997; Stock and Montgomery, 1999; Kühni and Pfiffner, 2001; Jansen *et al.*, 2010). Indeed, predictions from stream power-type models of fluvial erosion (e.g. Howard and Kerby, 1983; Whipple and Tucker, 1999) and field observations (e.g. Clayton and Shamoon, 1998; Clayton and Shamoon, 1999; Kühni and Pfiffner, 2001; Duvall *et al.*, 2004; Jansen *et al.*, 2010; Bursztyn *et al.*, 2015) both suggest that landscapes built in rocks with higher resistance to erosion will develop greater topographic relief, lower drainage densities, and steeper drainages when compared to those built in more erodible lithologies, assuming no variations in climate or uplift rates. It is also recognized that spatial variations in erodibility can cause discrete topographic features, with knickpoints often located at contacts between units with different bulk rock strengths, separating portions of the landscape with different local relief (Figure 1 e.g. Leopold and Bull, 1979; Miller, 1990; Goldrick and Bishop, 1995; Tooth *et al.*, 2002; Berlin and Anderson, 2007; Haviv *et al.*, 2010; Jansen *et al.*, 2010).

While the effect of rock erodibility on landscape form for spatially invariant patterns of rock strength is well known conceptually, the consequences of rock-contact migration during landscape evolution, and the resulting complex relationship between local rock erodibility and local erosion rates are much less widely appreciated and have not been systematically studied. Laboratory and short-term, outcrop-scale field measurements suggest a direct relationship between erosion rates and measures of rock strength or erodibility, with harder, less erodible rocks generally eroding more slowly (e.g. Sklar and Dietrich, 2001; Stock *et al.*, 2005; Marshall and Roering, 2014). In contrast, field analyses focused on larger-scale changes in landscape form emphasize that potential changes in geomorphology, e.g. development of local base levels at contacts between rocks with large strength contrasts, can dramatically influence the rate of incision of different parts of channels, potentially independent of the inherent rock strength (e.g. Leopold and Bull, 1979).

In Figure 1 we present a simple, conceptual model to illustrate the fundamental influence of lateral mobility of a single, horizontal contact between hard and soft rock layers. Specifically, we highlight the significance of the pace and pattern of landscape evolution and its consequences for spatio-temporal patterns of erosion rate and the relationship between local rock erodibility and local erosion rate (Figure 1). When an originally gentle, steady-state stream profile developed in easily eroded soft rock encounters the hard rock, the mouth of the stream will steepen to reach a gradient sufficient to continue incising at the uplift rate, while the upper reach will flatten as a stable local base level is developed (e.g. Leopold and Bull, 1979), imparting a spatially variable decrease in erosion rates upstream (Figure 1A, e.g. Darling and Whipple, 2015). Upstream of the contact in the soft over hard case, soft rock is eroded much slower than the hard rock downstream, and at a rate well below the rock uplift rate. Elsewhere both rock units are eroded at the rate of rock uplift. Contrastingly, in the case where hard rocks overlie soft rocks, when the originally steep gradient developed in the hard rocks exposes soft rock, the lower portion of the channel rapidly adjusts to lower slopes, undermining the upper portion of the channel and producing a steep, rapidly eroding knickpoint (Figure 1B). In this case, in the vicinity of the knickpoint both hard rocks and soft rocks

are eroded faster than the majority of the exposure of both rock types up and downstream of the knickpoint, and this time at a rate significantly exceeding the rock uplift rate.

In addition to the obvious implications of spatially variable erosion rates driven solely by contrasts in rock strength for assumptions of steady-state denudational conditions and the use of topography to explore changes in tectonics or climate, this concept also has broad implications for detrital records. Ages, abundances, and compositions of detrital minerals within both the ancient stratigraphic and modern sediment record provide key constraints for a range of geologic problems, including the first-order tectonic setting of ancient basins (e.g. Dickinson and Suczek, 1979; Bhatia, 1985; Myrow *et al.*, 2010; Cawood *et al.*, 2012), histories of structural development within orogenic systems (e.g. Garzanti *et al.*, 2004; Horton, 2005; Carrapa *et al.*, 2006; Bande *et al.*, 2012), changes in climate (e.g. Fedo *et al.*, 1995), major drainage network reorganizations (e.g. DeGraaf-Surpless *et al.*, 2002; Roddaz *et al.*, 2005; Cecil *et al.*, 2010; Wernicke, 2011), catchment-mean erosion rates (e.g. Bierman and Nichols, 2004), and histories of exhumation (Ruiz *et al.*, 2004; Ruhl and Hodges, 2005; Huntington and Hodges, 2006; Carrapa *et al.*, 2009; Carrapa, 2010). A base assumption embedded within the interpretation of most detrital records is that erosion rates do not vary significantly within the source area, thus assuming that the relative abundance of detrital minerals within a sediment sample derived from different contributing lithologies can be interpreted in terms of relative abundance of those lithologies within the landscape (Fedo *et al.*, 2003; Amidon *et al.*, 2005a; Stock *et al.*, 2006). When this assumption is violated and erosion rates vary within source areas, detrital records depart from predictions, introducing a potential bias in interpretation (e.g. DeCelles *et al.*, 1991; DeCelles *et al.*, 1993; Cawood *et al.*, 2003; Vezzoli *et al.*, 2004; Amidon *et al.*, 2005a; VanLanhingham *et al.*, 2008; Garretier *et al.*, 2015), but the effect of heterogeneous rock-strength within a source area on detrital records is largely unexplored.

Although, as outlined earlier, the spatial variation in erodibility due to different rock types intuitively would drive spatial variations in erosion rates (Figure 1), we are unaware of a systematic, quantitative assessment of the role of layered rocks in driving spatial and temporal variations in erosion rate and sediment sourcing. Additionally, while there has been previous theoretical work examining predicted changes in landscape form in response to variation in rock erodibility, these efforts were largely focused on randomly distributed heterogeneities (e.g. Moglen and Bras, 1995), processes at escarpments developed beneath a hard caprock (e.g. Howard, 1995; Haviv *et al.*, 2010; Ward *et al.*, 2011), or very specifically calibrated to particular field locations (e.g. Tucker and Slingerland, 1996; Cook *et al.*, 2009; Pelletier, 2010). To address this, our goal is to more generally explore the relationship between spatial variability in rock erodibility, geometry of contacts, landscape form, and related changes in erosion rates. To accomplish this, we use a version of the Channel-Hillslope Integrated Landscape Development (CHILD) model (Tucker *et al.*, 2001), LithoCHILD, which is modified to allow for spatial and temporal variability in erosional efficiency. We test a series of simple scenarios with two lithologies, a hard and soft rock, varying the relative order of these two units (i.e. hard rocks overlying soft and soft rocks overlying hard) and the magnitude of strength contrast between the hard and soft rocks. Next, we vary the dip of the contact between these two units with respect to the outlet of the streams draining the landscape. We then use the results of these models to calculate erosion rates of these two units through time to assess the extent to which (1) steady-state denudational conditions are achievable and (2) whether changes in landscape form and erosion rates might be reflected in detrital records.

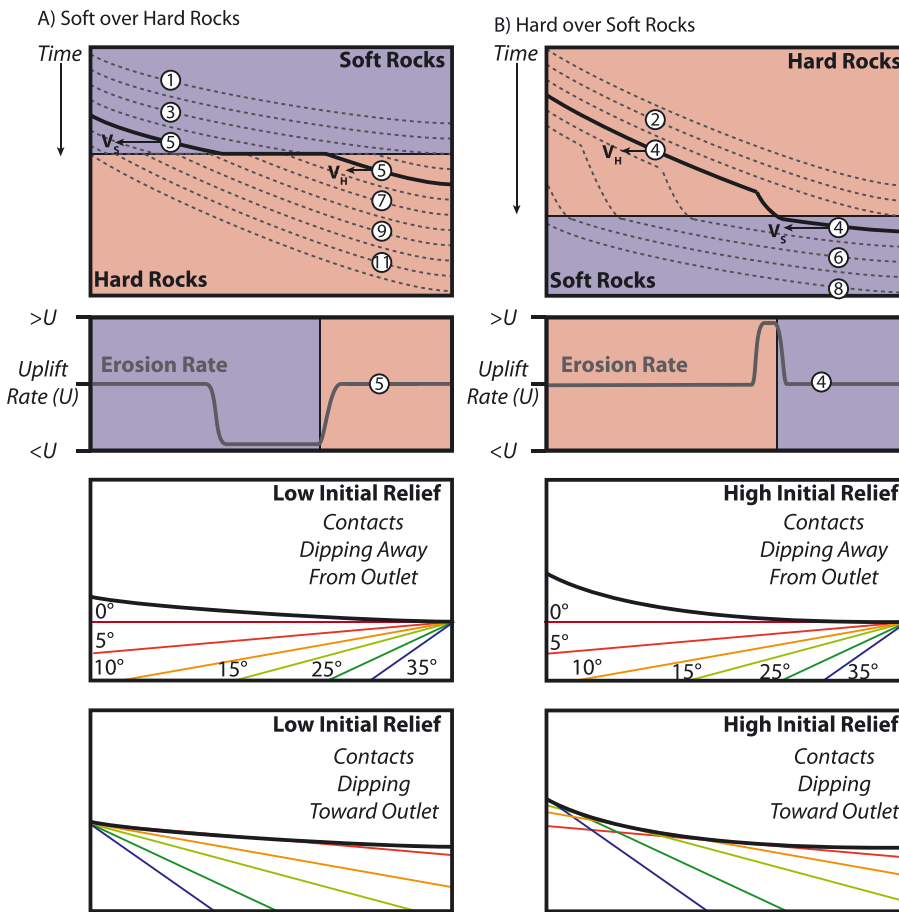


Figure 1. Conceptual model of a single channel's evolution and corresponding changes in erosion rates as it encounters a contact between (A) soft over hard rocks or (B) hard over soft rocks. Top panel shows channel longitudinal profiles through time with larger numbers indicating progression in time (i.e. the channel is incising downward toward and then through the contact). Horizontal arrows represent the relative speed at which channels migrate headward, highlighting that because of the contrast in rock strength (i.e. K), this velocity is faster in the soft rock (V_S) than in the hard rock (V_H). This ultimately leads to the differential evolution of the two profiles, where in the soft over hard case the portion of the river still within the soft rock is able to erode headward faster than the portion in the hard rock, developing a broad, nearly flat reach with a thin taper of the soft rock exposed. In contrast, in the hard over soft rock case, the faster headward erosion of the underlying soft rock portion essentially undermines the upstream portion, producing an over-steepened reach mostly formed in the hard rock just upstream of the contact. The second panel from the top shows predicted patterns in erosion rates for the time step marked in bold in the top panel, plotted relative to the background constant uplift rate. See text for additional discussion. The two bottom panels illustrate how the earlier mentioned scenario can be further complicated if the contact between the two rock strengths is dipping. In cases where the contact is horizontal or dipping away from the outlet, the underlying rock unit will always be exposed at the outlet, but in the case of a contact dipping toward the outlet, the first exposure of the underlying rock unit can occur at the top, bottom, or middle of the channel as dictated by river slope relative to contact dip. This figure is available in colour online at wileyonlinelibrary.com/journal/espl

Methods – Landscape Evolution Modeling

We employ the CHILD model (Tucker *et al.*, 2001) to simulate landscape evolution. To model spatially and temporally variable lithology, modifications were made to the CHILD code to allow the landscape to develop over any three-dimensional (3D) geologic model. We refer to this modified version as LithoCHILD, see Supporting Information for additional discussion. In all of the models presented here, we only vary fluvial bedrock erodibility keeping all other values constant between all units in all model runs.

All models are set up such that they drain from one side (bottom in all figures and $Y=0$) with the other boundaries closed (water cannot flow out, but can flow along the boundary toward the outlet) and are 40 km wide by 20 km long with an average node spacing of 100 m. The uplift rate is uniform and steady at 1 mm yr^{-1} for all models. We assume a simple detachment limited model with uniform precipitation, equivalent to 1 myr^{-1} mean annual precipitation, and an initial topography initialized with the same random seed so that all models have the same starting channel network. Hillslope processes

are modeled as simple linear diffusion and a diffusion coefficient of $1.0 \times 10^{-5} \text{ m}^2 \text{ yr}^{-1}$ is used in all model runs and units, though more generally LithoCHILD supports variable diffusion constants between different units (see Supporting Information). Within the model, fluvial incision rate (ε) is calculated as a function of unit stream power, such that:

$$\varepsilon = k_b \left(\frac{Q}{W} \right) S \quad (1)$$

where Q is discharge, W is channel width, S is slope, and k_b is the fluvial erodibility parameter that varies between units. Note that the values of k_b discussed in the text and as used in the model include values for gravitational acceleration and the density of water. Combined with empirical descriptions of hydraulic geometry and basin hydrology (Equation 1) is consistent with the well-known stream power model (Whipple and Tucker, 1999):

$$\varepsilon = KA^m S^n \quad (2)$$

where K is a dimensional coefficient of erosional efficiency (linearly dependent on k_b), A is drainage area as a proxy for discharge, S is slope and m and n are positive constants which are effectively set to 0.5 and 1 within the models, respectively. These values for m and n are based on the theoretical prediction and empirical observation that the ratio of m/n should be ~0.5 and that $n=1$ is a simple case where erosion is linearly proportional to shear stress (e.g. Whipple and Tucker, 1999, 2002). The erosional efficiency K in the stream power model incorporates effects from the substrate (e.g. bedrock erodibility), climate, and hydrology. Because we hold all other parameters fixed through time and between models, the imposed spatial variability in k_b can be interpreted as spatial variability in K and for simplicity we refer to variations in k_b as variations in K throughout. Models have a time-step of 1000 years with an output every 100 kyr.

Three main contact geometries are tested; horizontal, dipping away from the outlet, and dipping toward the outlet. For the dipping models, dips of 5°, 10°, 15°, 25°, and 35° are tested, but we primarily discuss the 5° and 35° models as the results from the intervening models are largely gradational between these two. Each model geometry is run with both a soft over hard rock and hard over soft rock case. The K value for the soft rock is held fixed at $1.0 \times 10^{-5} \text{ yr}^{-1}$, and K values of 0.1, 0.2, 0.3, 0.4, and $0.5 \times 10^{-5} \text{ yr}^{-1}$ are used for the hard rock in horizontal models and K values of 0.2, 0.3, and $0.4 \times 10^{-5} \text{ yr}^{-1}$ are used for the hard rock in all dipping models. The absolute values of K in natural settings are poorly constrained and will also depend on the choice of exponents in Equation 2. Results of experiments and field investigations suggest that K values may span up to five-orders of magnitude (e.g. Stock and Montgomery, 1999; Sklar and Dietrich, 2001; Bursztyn et al., 2015), compared to the one-order of magnitude we use here. In detail, after correcting for different values of m and n , the magnitudes we use for K are within the lower range of K values (i.e. harder rocks) reported by Stock and Montgomery (1999). We focus our discussion of results on models that use $0.2 \times 10^{-5} \text{ yr}^{-1}$ as the K value for the hard rock (a factor of five less erodible than the soft rock), but also briefly consider the effect of changes in strength contrast (hard rock 2–10 times less erodible than soft rock).

Details of the landscape evolution in cases with horizontally dipping contacts and those with contacts dipping at 5° and 35° both toward and away from the outlet are described in the following. Beginning in panel A of Figures 2–10, we present selected time-slices from these models illustrating the distribution of the two units (top panels) and erosion rates (lower panels). We also include 10 km wide swath profiles (mean, minimum, and maximum values), oriented perpendicular to the open boundary, to illustrate topography and the spatial distribution of erosion rates at the selected time steps (middle panel). We also consider changes in average erosion rates measured across the entire landscape and within individual rock units through time along with changes in the areal distribution of the two units with time.

Many of the changes in landscape form and erosion rates are easiest to visualize as animations, so within the Supporting Information we provide time series of the distribution of units, elevation, erosion rates, and a 10 km wide topographic swath profile across the model length for all the models discussed. In the animations we refer to the K value of the overlying, or initial, rock as K_i and the K value of the underlying, or final, rock as K_f . Within the Supporting Information, we additionally show the evolution of river profiles both as elevation-distance plots and elevation-chi plots, showing mainstem and tributaries from the largest catchment in the model. Chi-elevation plots are useful in assessing the degree to which a river profile is in

equilibrium, with straight lines on chi-elevation plots indicating an equilibrium profile (for uniform lithology, climate, and uplift rate) and higher slope values indicating higher channel steepness index values (e.g. Harkins et al., 2007; Perron and Royden, 2013), where chi (χ) is an integral evaluated such that:

$$\chi = \int_{x_b}^x \left(\frac{A_0}{A(x)} \right)^{\theta_{ref}} dx \quad (3)$$

and x_b is the position of the river mouth, x is position along the channel, $A(x)$ is drainage area as a function of distance along the profile, A_0 is a reference drainage area, such that if this reference value is set to 1 km² (if drainage area is measured in km²) then the slope of a chi-elevation plot is equal to the normalized channel steepness index, and θ_{ref} is a reference concavity, equivalent to the ratio of m/n in Equation 1. River profiles and chi values were calculated from model results using TopoToolbox with a reference area of 1 km² and a reference concavity of 0.5 (Schwanghart and Scherler, 2014). Throughout the Results, times within the model results are reported as time since first exposure of the underlying unit.

Results

Soft rocks over hard rocks

Horizontal contacts

Models with soft rocks overlying hard rocks across a horizontal contact initially develop a low-relief landscape prior to exposure of the hard rocks (Figure 2-A2 and Supporting Information Movie S1). The hard rock is first exposed at the outlet ($Y=0$), forming an initial higher relief area and a knickpoint at the contact as the profiles of rivers within the hard rock steepen as rock-uplift outpaces erosion (Figures 1A and 2-B2, Supporting Information Figures S1D and S1E). Note that as they are exposed, the hard rocks are eroded as fast as were the soft rocks ($E=U$), but the landscape steepens where hard rocks are exposed. The adjustment of individual channels, and the landscape as a whole, to the exposure of the underlying hard rock is analogous to channels adjusting to a change in the rate of base level fall. In the case of a change in the rate of base level fall, the information is communicated upstream at a rate well described by a kinematic wave equation (e.g. Rosenbloom and Anderson, 1994; Whipple and Tucker, 1999):

$$C_e = -KA^mS^{n-1} \quad (4)$$

where C_e is the wave speed. In the simple case where n equals 1, as it does in our models, the rate at which the kinematic wave propagates upstream (C_e), is a function of K and drainage area alone, where a smaller K , i.e. harder rocks, yields slower rates of propagation. Applying this concept to the models, we can consider the two parts of any given stream profile developed within the two rock units as two separate kinematic waves with different propagation speeds (Figure 1A). This is possible because at any given point along the network, which has the same drainage area, the rate of propagation is faster within the overlying soft rocks. However, incision into soft rocks cannot cut deeper than the downstream reach incising hard rocks such that the top of this downstream reach establishes a stable local baselevel for all points upstream. As channels within the soft rocks continue to erode rapidly headward and the wave speed of the soft-rock segment continues to outpace that in the hard-rock segment, a plateau bench often preserving a thin layer of the soft rock forms and

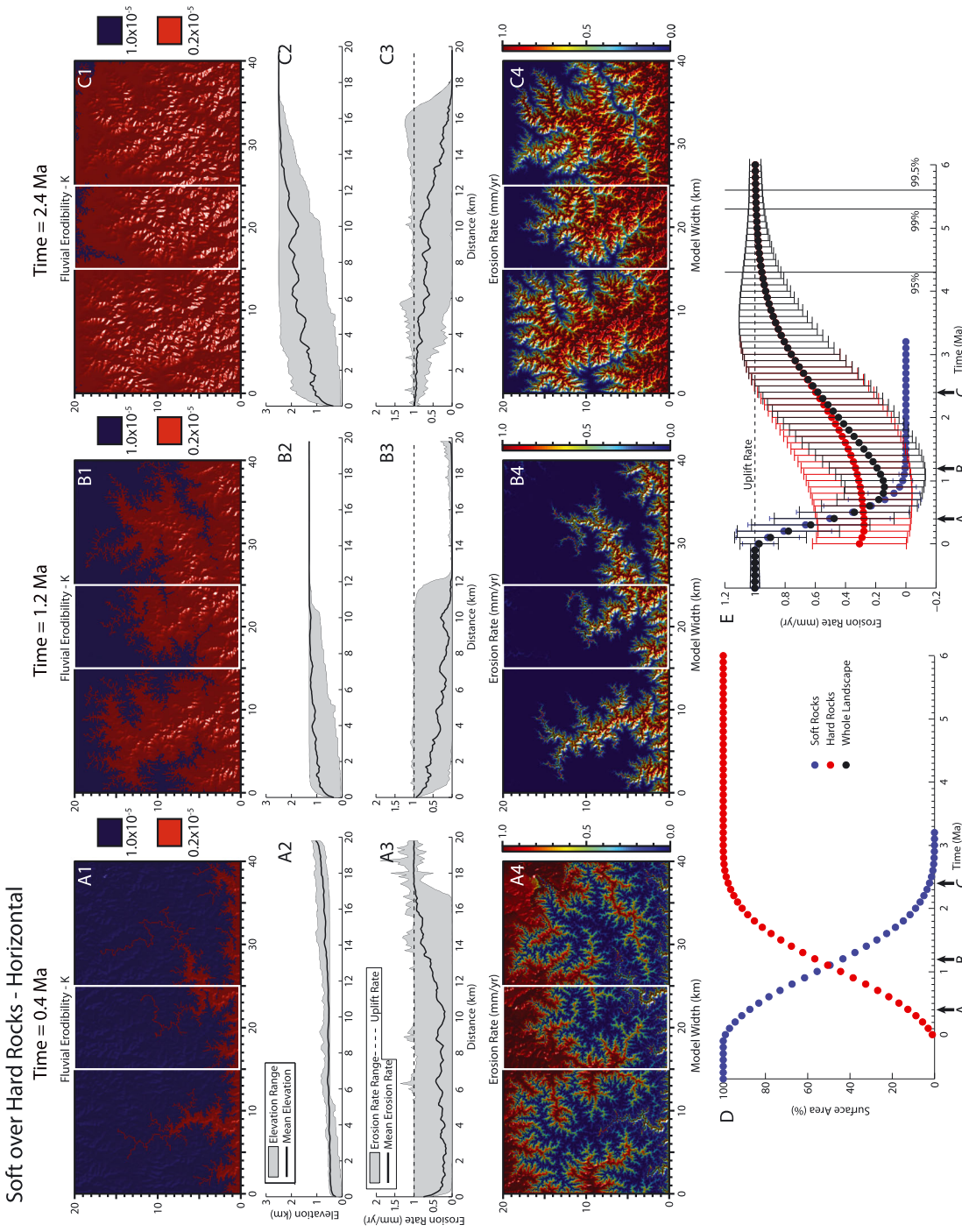


Figure 2. Selected results from three time steps (A, B, and C) of the soft over hard model with a horizontal contact and a hard rock K value of $0.2 \times 10^{-5} \text{ yr}^{-1}$ and a soft rock K value of $1.0 \times 10^{-5} \text{ yr}^{-1}$. Time within the models is measured in millions of years since the first exposure of the underlying unit. Each time step includes a shaded relief map colored by rock erodibility (A1, B1, and C1), a 10 km wide topographic swath profile oriented parallel to model length (white box in map figures indicates swath location) showing mean elevation in black and maximum and minimum elevations within the gray shaded region (A2, B2, and C2), a swath of erosion rates, co-located with the topographic swath, illustrating mean erosion rate with the black line and minimum and maximum erosion rates within the gray shaded region (A3, B3, and C3), and a shaded relief map colored by erosion rate (A4, B4, and C4). For all map figures, the outlet of the model is along the bottom of the frame. Panel D is a graph of the percentage of area represented by the hard (red) and the soft (blue) rock through time. Panel E shows average and $1 - \sigma$ of the standard deviation of erosion rates measured from the entire landscape (black), from just the hard rock (red), and from just the soft rock (blue). Vertical black lines in E indicate the time required for the average erosion rate to return to values 95%, 99%, and 99.5% of the uplift rate. Positions of the time steps in panels A, B, and C are marked in D and E. Additional results from this model are presented in Supporting Information Movie S1 and Figure S1. This figure is available in colour online at wileyonlinelibrary.com/journal/espl

widens with time at this local baselevel and relief in the soft-rock covered landscape upstream of the contact is progressively reduced (Figures 1A and 2, and Supporting Information Figure S1). As the relief within the soft rock portion of the landscape decreases, so does the erosion rate, thus the average erosion rate of the landscape upstream of canyons incising into the hard rocks drops below the uplift rate (Figures 1A and 2E). Where the rivers are actively incising into hard rock, erosion rate is set by the uplift rate. Consequently, the hard rock erodes at a faster rate than the soft rock throughout most of the model run (Figure 2E). In detail, the majority of the landscape within the hard rock erodes at a rate near the uplift rate, but the upper reaches of the hard rock just below the stripped away soft rocks erosion rates are low as the lingering low-relief landscape developed in the soft rocks persists and the extremely low slope thus dictates the erosion rates (Figure 2C). Time evolution of chi-z plots highlight the disequilibrium that characterizes these models, with significant portions of the channel profiles having a near zero slope, indicating extremely low channel steepness values (Supporting Information Figure S1D). Once the soft rock is completely eroded away and the knickpoints have propagated to the top of the model domain, the entire landscape approaches steady state with the average erosion rate again approaching the uplift rate (Movie S1).

Shallowly dipping (5°) contacts

As the orientation of the contact changes, so do the patterns in landscape evolution and erosion rates. At low dips oriented away from the outlet, e.g. 5° , soft over hard models behave relatively similarly to their horizontal equivalents, but with some important differences (Figure 3). The hard rock is still first exposed at the outlet, with a knickpoint forming in the underlying hard rock unit that propagates toward the imposed drainage divide (Figures 1A and 3, Movie S2). Importantly though, in the soft over hard, shallowly dipping away models, the low relief plateau that develops in the overlying soft rocks is not as extensive, and similarly, erosion rates do not drop as much on this plateau as in the horizontal models (Figure 3, Movie S2). Because the soft/hard contact dips upstream, the local baselevel set by the knickpoint at upstream lip of canyons incised into hard rock is no longer stable, but rather falls at a rate set by the dip of the contact and the kinematic wavespeed of the hard-rock section (Cook *et al.*, 2009), thus increasing erosion rates upstream compared to the case with a horizontal contact. This can be seen in chi-z plots as well, where channel steepnesses within the soft rock portion of the landscape are higher in the 5° case (Supporting Information Figure S2C) than in the horizontal case (Supporting Information Figure S1D). Also, while canyons do form in the hard rocks, they do not persist as long as in the horizontal case. This leads to a less dramatic difference between the erosion rates of the hard and soft rocks, but crucially, average rates remain below the uplift rate and the hard rocks, on average, erode faster than the soft rocks until the soft rocks are removed and the entire landscape approaches steady state (Figure 3D).

The landscape evolution of models in which strata dip toward the outlet fundamentally differ from both the horizontal and dipping away models because the underlying unit is generally not first exposed at the outlet, but instead appears higher in the landscape (i.e. closer to the drainage divide). Where the underlying unit is first exposed depends primarily on the relief of the pre-existing landscape, which is dictated by the rock uplift rate, K , and the dip of the contact (Figure 1). In the case of soft over hard rocks with a 5° dip toward the outlet, because of the low relief of the initial landscape, the underlying soft rocks are first exposed near the drainage divide (Figures 1A and 4). Thus, the contact between the

overlying soft and underlying hard rocks propagates downstream toward the outlet (Figure 4, Movie S3). Because the slope of the original landscape developed in the soft rock is similar to the slope of the contact, a shallow dip-slope forms in the hard rock, with the contact essentially moving down this dip-slope. The contact represents a local, falling base level for the portions of the rivers within the hard rock, but also a base level that is moving downstream at a similar rate to uplift, such that no steepening of the landscape occurs. The depressed slopes coupled with the harder rocks, leads to a decrease in erosion rates within the upper portion of the landscape (Figure 4, Movie S3). It is not until the soft rock is entirely removed from the landscape that channels within the hard rock begin to respond to a rate of base level fall equal to the rock uplift rate and thus begin to steepen. Erosion rates at or near the uplift rate thus sweep upstream as in cases with no dip or a gentle dip away from the outlet (Figure 4C4, Figure S3 and Movie S3).

Steeply dipping (35°) contacts

As the dip of the contact increases, the contact itself becomes an important topographic feature, and as a result, imparts significant changes in the patterns of erosion rates. In soft over hard rocks, with the contact dipping away from the outlet, the exposure of the underlying hard rock produces a prominent, slowly eroding, uphill facing dip slope that forms along the upstream edge of the hard rock exposure, and which then propagates away from the outlet toward the imposed drainage divide (Figure 5, Movie S4). This means that within the model domain, the highest relief and elevation portion of the landscape develops near the outlet and propagates toward the drainage divide. The erosion rates downstream of the contact and the prominent uphill facing dip-slope remain near the uplift rates, but erosion rates are suppressed upstream of the contact as the dip-slope imposes a reduced rate of base level fall affecting both upstream reaches of these channels, but also the channels forming on the dip slope itself (e.g. Figure 5A4, Movie S4). Most clearly demonstrated in the animation of the landscape evolution of this model (Movie S4), the depression of erosion rates within catchments upstream of the contact leads to cannibalization by neighboring drainage basins still eroding at rates closer to the uplift rate via divide migration. At the landscape scale, this pattern leads to a scenario early in the run where the soft rocks erode at near the uplift rate, but the average erosion rates for the hard rock are depressed below the uplift rate (Figure 5D). This pattern reverses later in the run as more of the soft rock landscape is dominated by isolated regions of local base level and more of the hard rock landscape has reached steady state (Figure 5B4).

When the contact between soft and hard rocks dips toward the outlet, the hard rock is first exposed near the drainage divide (Figures 1A and 6). The contact between the two units propagates downstream, toward the outlet. Similar to the model where the contact dips away, a prominent, slowly eroding dip slope forms within the hard rock at the contact between the soft and hard rock, but importantly, the dip-slope faces downstream (Figure 6, Movie S5). The soft rocks erode at the uplift rate throughout the model run, but because of the slowly eroding dip-slope, the average erosion rate of the hard rocks is consistently lower than the uplift rate (Figure 6D).

Hard rocks over soft rocks

Horizontal contacts

The landscape evolution of models with hard over soft rocks fundamentally differ from the preceding models with soft rocks

Soft over Hard Rocks - Dipping Away 5°

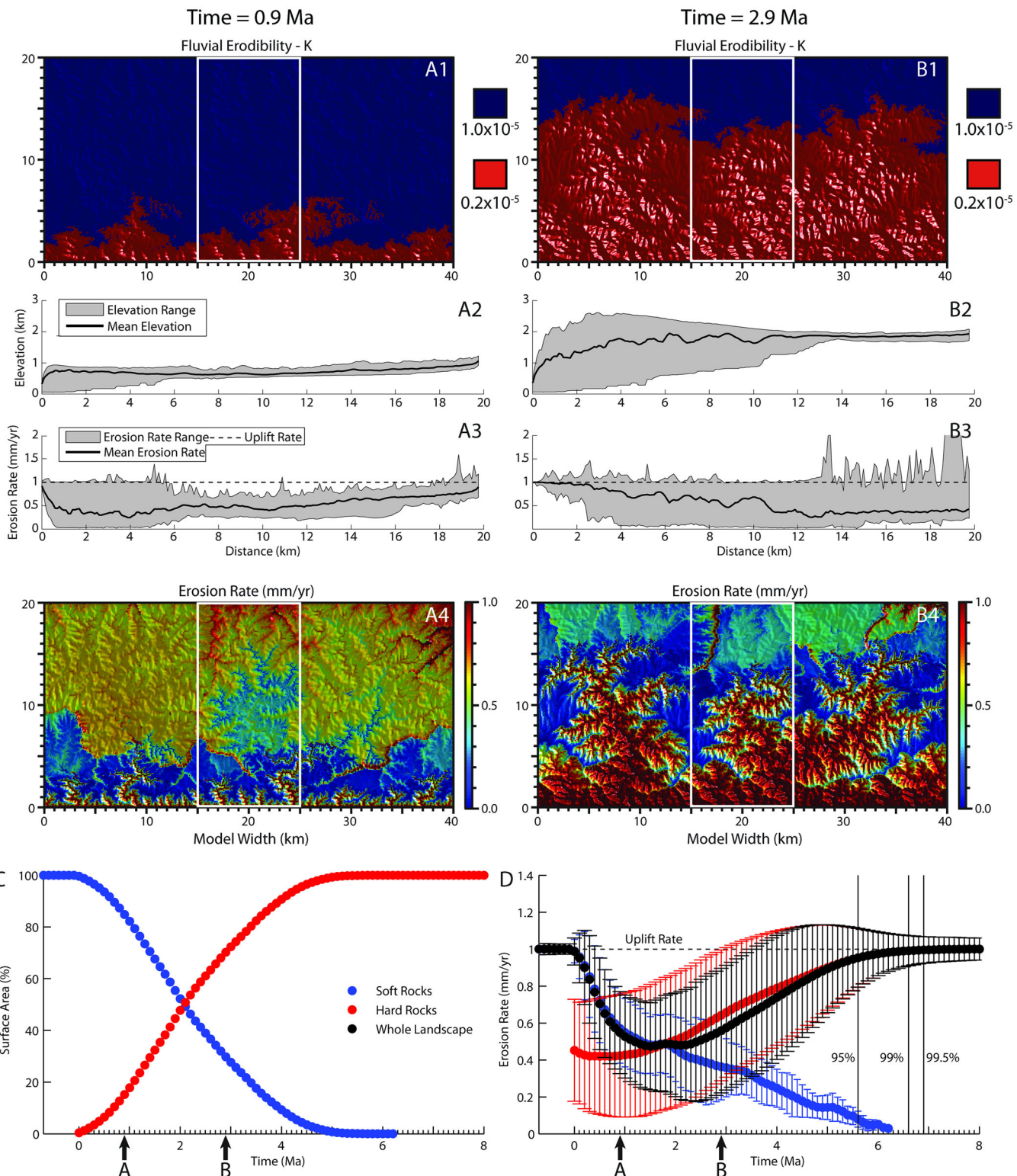


Figure 3. Selected results from two time steps (A and B) of soft over hard model with a contact dipping 5° away from the outlet, a hard rock K value of 0.2×10^{-5} yr $^{-1}$, and a soft rock K value of 1.0×10^{-5} yr $^{-1}$. Setup for this figure is the same as in Figure 2. See Supporting Information Movie S2 and Figure S2 for additional results from this model. This figure is available in colour online at wileyonlinelibrary.com/journal/espl

overlying hard rocks. First considering models with a horizontal contact, when the soft rock is first exposed at the outlet of the model, a low relief region quickly develops (Figures 1B and 7A). As was the case for the soft over hard scenario, landscape evolution of the horizontal hard over soft rock model can be explained best in the context of the propagation rates of kinematic waves (Equation 4) within the two portions of the

landscape (Figure 1B). The faster rate of propagation within the underlying soft rock with respect to the overlying hard rock, coupled with the requirement that the channel remain continuous, leads to an oversteepening (steepening to greater than the steady-state slope) of river profiles near the contact between the hard and soft rock (Figure 1B); erosion of the soft rock is undermining the overlying hard rock. This is manifest in the

Soft over Hard Rocks - Dipping Toward 5°

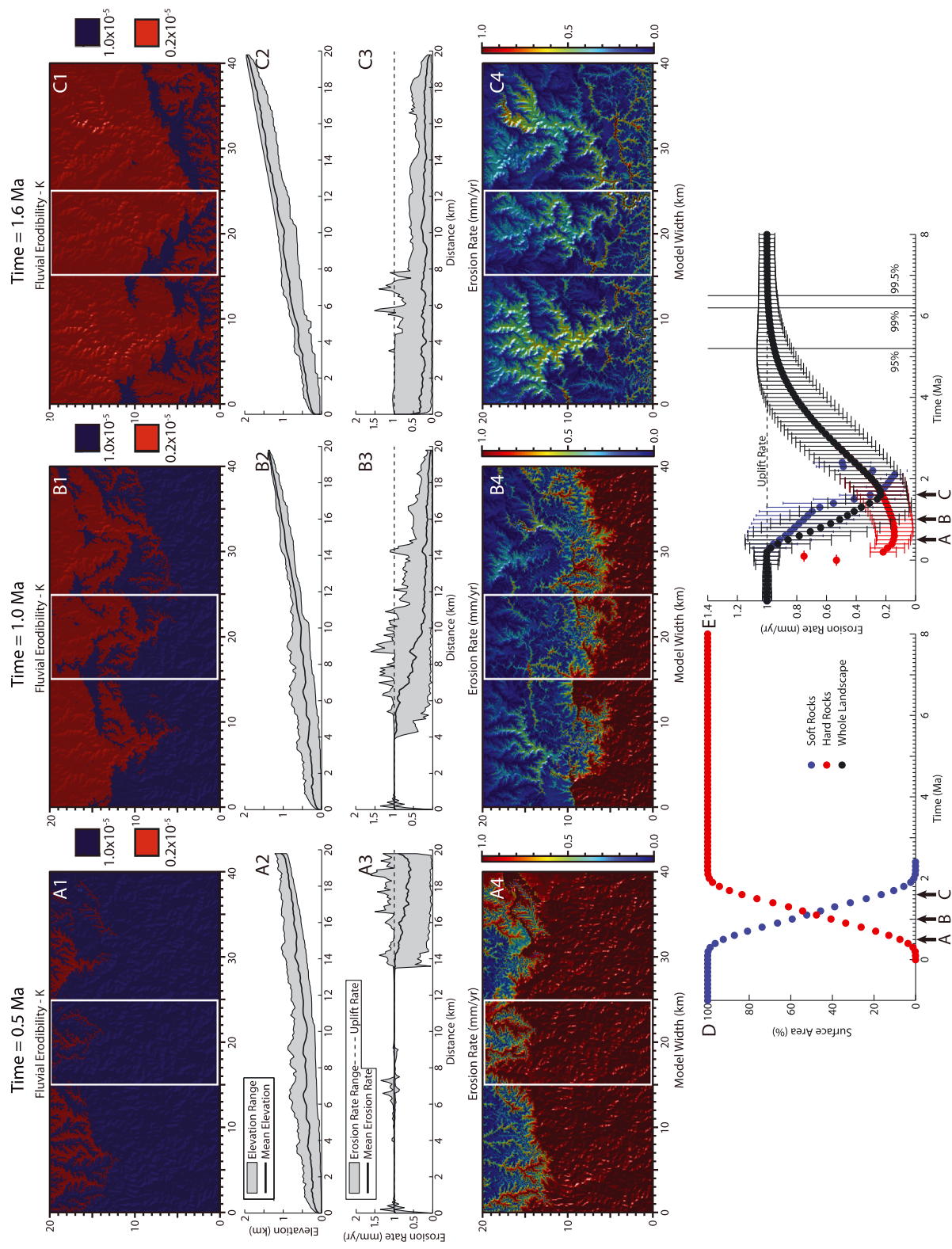


Figure 4. Selected results from three time steps (A, B, and C) of soft over hard model with contact dipping 5° toward the outlet, a hard rock K value of $0.2 \times 10^{-5} \text{ yr}^{-1}$, and a soft rock K value of $1.0 \times 10^{-5} \text{ yr}^{-1}$. Setup for this figure is the same as in Figure 2. See Supporting Information Movie S3 and Figure S3 for additional results from this model. This figure is available in colour online at wileyonlinelibrary.com/journal/espl

Soft over Hard Rocks - Dipping Away 35°

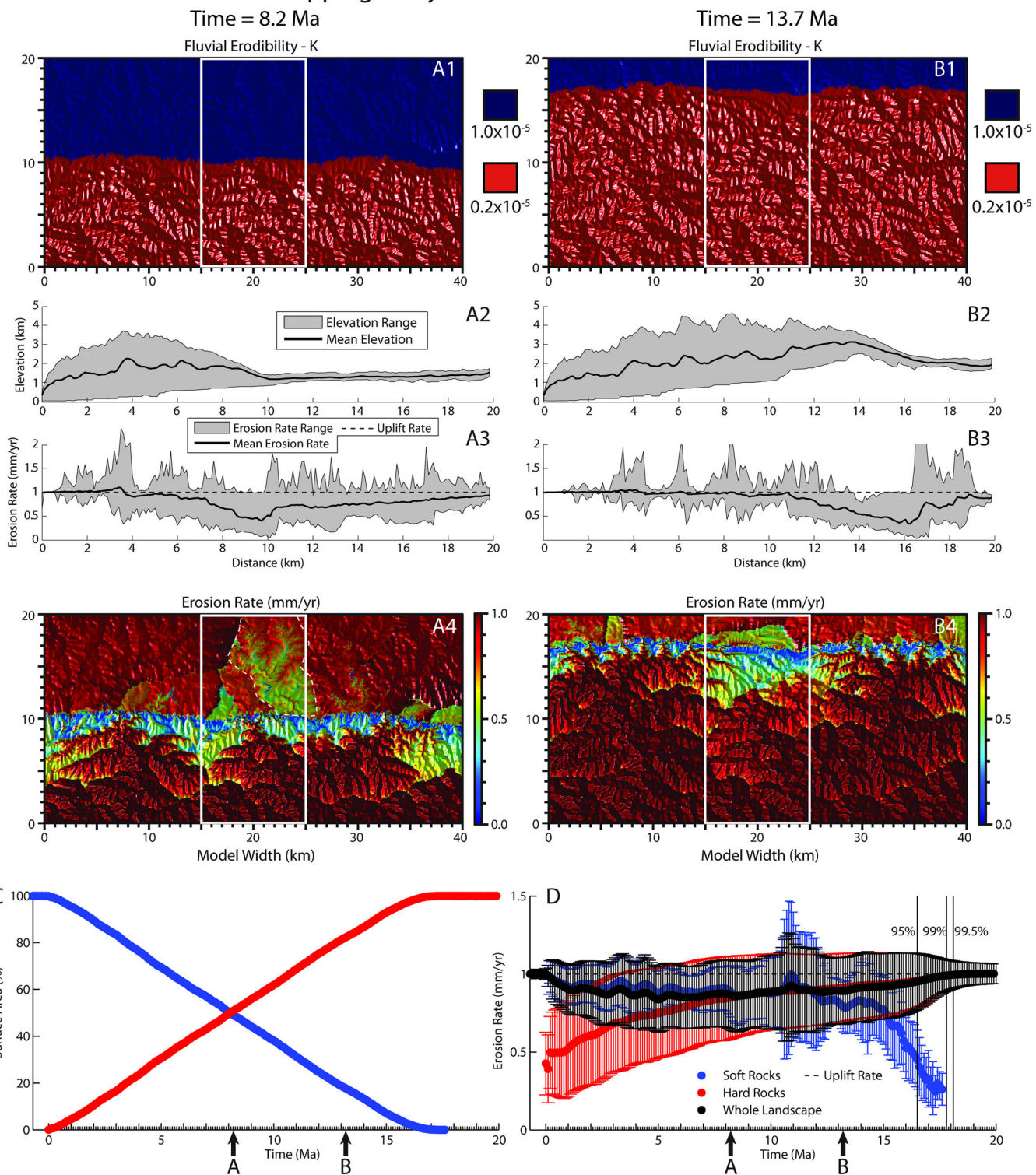


Figure 5. Selected results from two time steps (A and B) of soft over hard model with contact dipping 35° away from the outlet, a hard rock K value of 0.2×10^{-5} yr $^{-1}$, and a soft rock K value of 1.0×10^{-5} yr $^{-1}$. Setup for this figure is the same as in Figure 2. See Supporting Information Movie S4 and Figure S4 for additional results from this model. White dashed line in A4 outlines area of depressed erosion rate described in the main text. This figure is available in colour online at wileyonlinelibrary.com/journal/espl

model topography as an abrupt scarp separating the high relief landscape developed in the overlying hard rock and the low relief landscape developed in the underlying soft rock and a pronounced convex-up, slope-break knickpoint developed within the hard rock (e.g. Figure 1B, Supporting Information Figure S6E). Chi-z plots accentuate the discrete zone of extremely high channel steepness localized near the contact, significantly higher than that developed in either the soft or hard rocks (Supporting Information Figure S6D). This scarp and knickpoint

propagate headward toward the drainage divide of the model (Figure 7, Figure S6D and Movie S6).

The majority of both the hard and soft rock portions of the landscape erode at rates near the uplift rate, but in the vicinity of the scarp, erosion rates significantly exceed the uplift rate (Figures 1B and 7-B4, Movie S6). Because of the oversteepened slope of the escarpment, this portion of the landscape erodes at rates significantly above the uplift rate, bringing the average erosion rates for the landscape as a whole above the uplift rate

Soft over Hard Rocks - Dipping Toward 35°

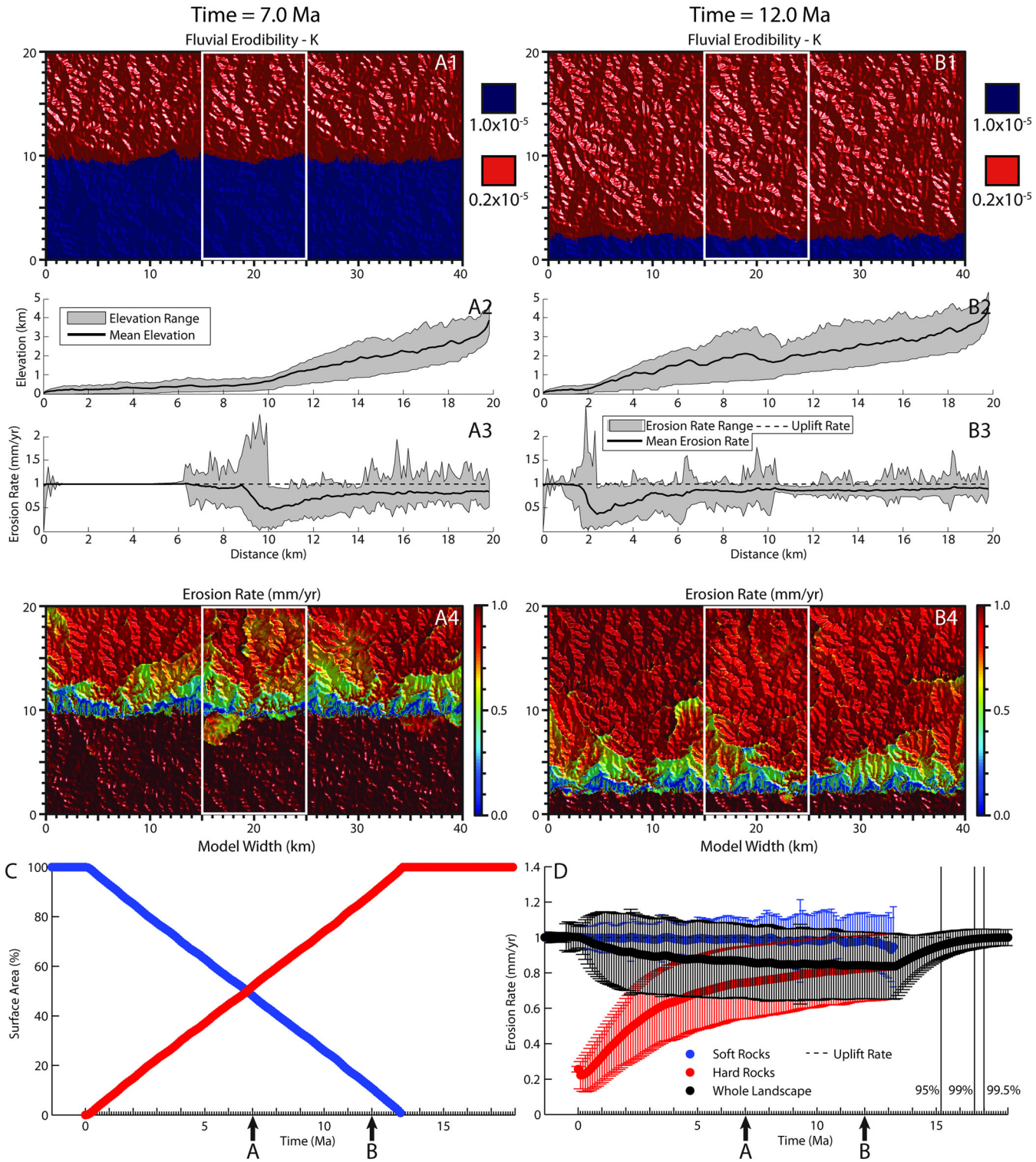


Figure 6. Selected results from two time steps (A and B) of soft over hard model with contact dipping 35° toward the outlet, a hard rock K value of 0.2×10^{-5} yr. $^{-1}$, and a soft rock K value of 1.0×10^{-5} yr. $^{-1}$. Setup for this figure is the same as in Figure 2. See Supporting Information Movie S5 and Figure S5 for additional results from this model. This figure is available in colour online at wileyonlinelibrary.com/journal/espl

(Figure 7E). This region of elevated erosion rates associated with knickpoint and scarp is primarily developed in the hard rock, but erosion rates within the upper portions of the soft rock, at the base of the escarpment, are also elevated (Figures 1B and 7). This region of high erosion rates propagates with the knickpoint toward the drainage divide of the model and as the portion of the landscape represented by the hard rock decreases (Figure 7D), the average erosion rates of the

hard unit increase significantly above the uplift rate as the rapidly eroding escarpment represents more of the total landscape area of the hard unit (Figure 7E).

Shallowly dipping (5°) contacts

For models with hard over soft rocks and contacts dipping shallowly (e.g. 5°) away from the outlet, the propagation of the contact (Supporting Information Figures S7 A1 and S7 B1),

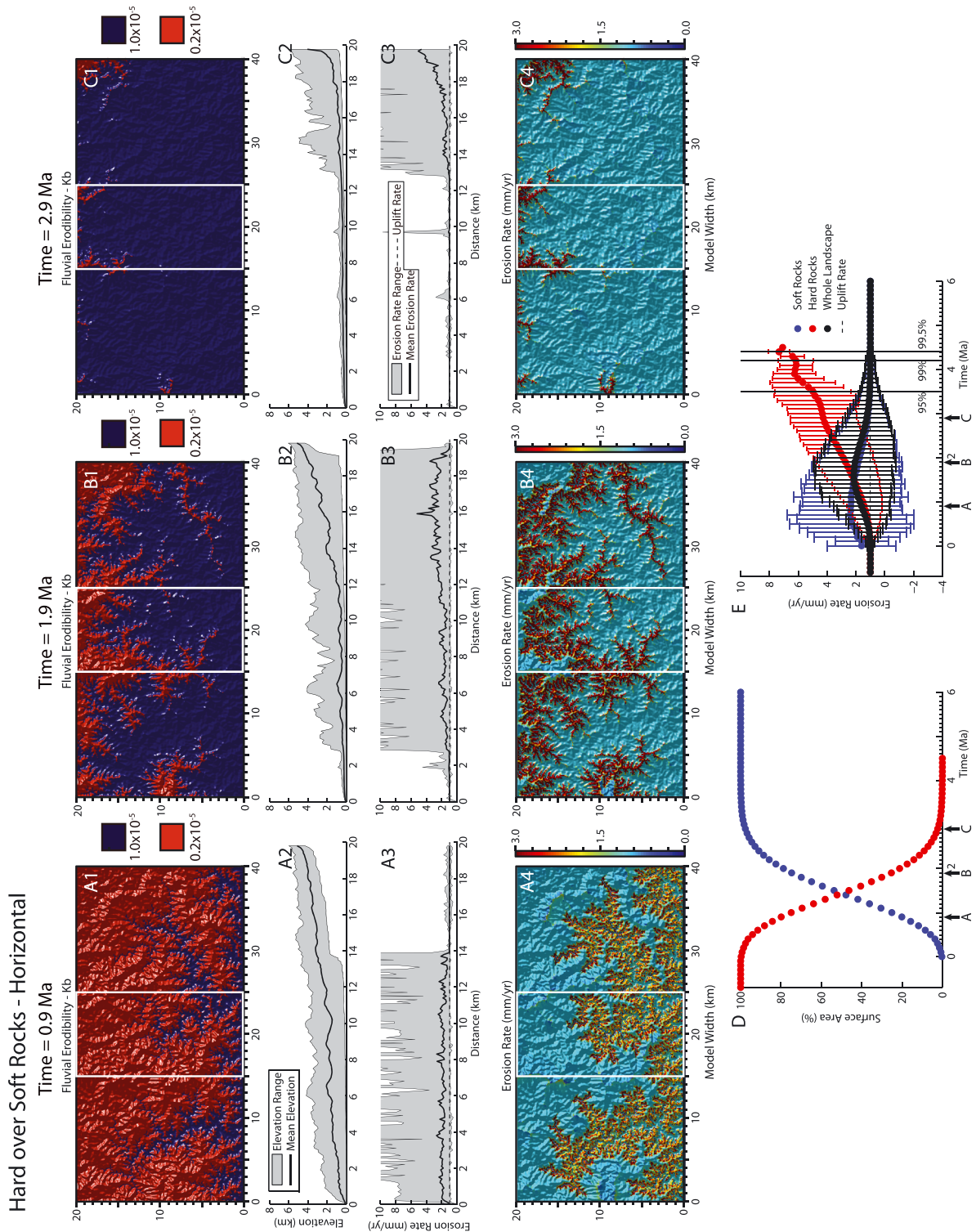


Figure 7. Selected results from three time steps (A, B, and C) of hard over soft model with a horizontal contact, a hard rock K value of $1.0 \times 10^{-5} \text{ yr}^{-1}$, and a soft rock K value of $0.2 \times 10^{-5} \text{ yr}^{-1}$. Setup for this figure is similar to Figure 2, but the scales for the erosion rate swath (A3, B3, and C3), erosion rate with time (E), and erosion rate with time (E) are increased to reflect that maximum erosion rates within hard over soft models often locally reach values significantly greater than the uplift rate (1 mm yr^{-1}). Also note that for the erosion rate swath (A3, B3, and C3), the graph only extends to 10 mm yr^{-1} , but isolated nodes within the model domain frequently greatly exceed 10 mm yr^{-1} , hence the apparent cutoff of the erosion rate swath. The fact that the mean erosion rates, indicated with the black line, generally remain significantly lower than 10 mm yr^{-1} indicates that these high values are indeed isolated. See Supporting Information Movie S6 and Figure S6 for additional results from this model. This figure is available in colour online at wileyonlinelibrary.com/journal/espl.

Hard over Soft Rocks - Dipping Toward 5°

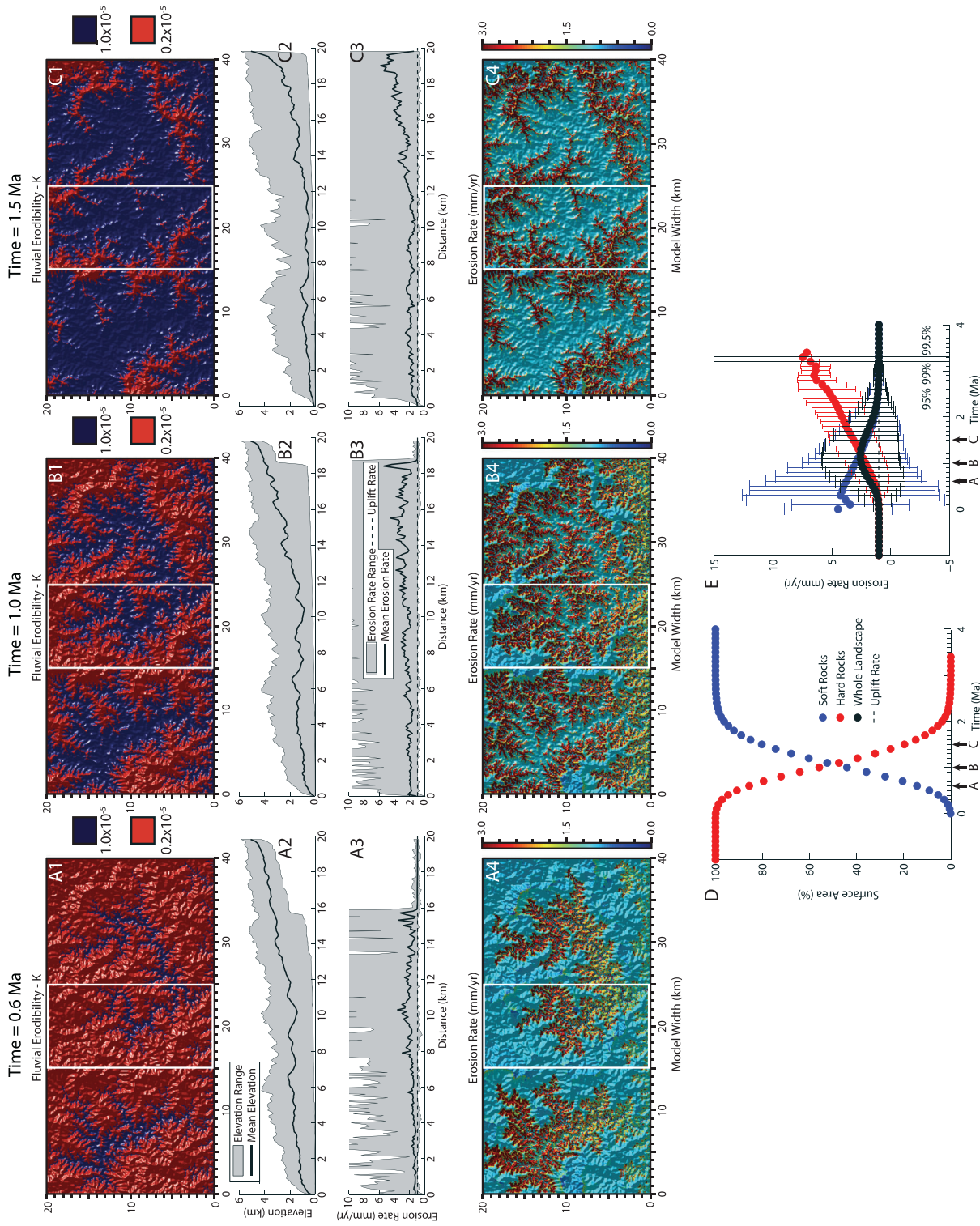


Figure 8. Selected results from three time steps (A, B, and C) of hard over soft model with a contact dipping 5° toward the outlet, a hard rock K value of 0.2×10^{-5} yr $^{-1}$, and a soft rock K value of 1.0×10^{-5} yr $^{-1}$. Setup for this figure is the same as in Figure 7. See Supporting Information Movie S8 and Figure S9 for additional results from this model. This figure is available in colour online at wileyonlinelibrary.com/journal/espl

topographic form (Figures S7 A2 and S7B2), and patterns in erosion rates (Figures S7A4, S7B4, and S7E) are all largely indistinguishable from the horizontally bedded hard over soft model (Figure 7, Movies S6 and S7). In contrast, 5° contacts that dip toward the outlet differ because the underlying soft rock is first exposed near the center of the landscape (Figures 1B and 8). It is important to reiterate that the location of contact exposure results from the combined influence of the relief, which is dictated by the uplift rate and the initial value of K , and the dip, so models or natural landscapes with different values of K or uplift rate and a 5° dipping contact may have initial exposure of the contact in places other than the center of the landscape. The landscape form developed near this contact is largely similar to that observed with contacts horizontal to dipping shallowly away (Figure 7, Figure S7), namely a steep, rapidly eroding scarp developed primarily within the hard rock, but hard contact dips upstream rock is first exposed in the deepest stream valleys in the middle of the landscape, scarps form in canyon walls along middle sections of the largest catchments and then propagate out radially (Figure 8, Movie S8). This means that while the patterns in average landscape erosion rates are largely the same as in the horizontal and dipping away models, the time required for the model to return to a state where erosion equals uplift rate is decidedly shorter (Figures 7E, 8D, and 8E).

Steeply dipping (35°) contacts

Increasing dips in hard over soft models result in very linear contacts with narrow bands of high erosion rates localized near these contacts (Figures 9, 10). The high erosion rate bands result from the same scarp developed in models with more gently dipping contacts and for the same reasons. Unlike in the horizontal or shallow dipping contact scenarios however, the scarp is narrow enough that no significant over-steepened zone is evident in chi-z plots (Supporting Information Figures S10 and S11). Dip direction influences the propagation direction of both the contact and this localized zone of fast erosion. The underlying soft rocks are first exposed near the outlet if the contact dips away from the outlet, and thus the contact and band of high erosion rates propagate upstream toward the drainage divide (Figure 9, Movie S9). In contrast, because the initial high relief developed in the overlying hard rocks, when the contact dips toward the outlet, the soft rocks are first exposed at the drainage divide (Figures 1B and 10) and thus the contact and band of high erosion rates within the hard rocks propagate downstream toward the outlet. Regardless of dip direction, because of the extremely localized nature of the scarp in models with steeply dipping contacts and hard over soft rocks, deviations in average erosion rates only occur when the eroding scarp makes up the bulk of the landscape area of a given unit (Figures 9C, 9D, 10C, and 10D).

Magnitude of rock strength contrasts

Decreasing contrasts in rock strength, i.e. increasing the absolute value of the hard rock K , decreases both the magnitude of the deviation of erosion rates from uplift rate and the duration of this deviation (Figures 11, 12). Examining the same time-slice, i.e. the same time since the initial exposure of the contact, for five different K values for the hard rock in the horizontally bedded, soft over hard rock case is instructive for general patterns in changes in the effect of magnitude of K contrast (Figure 11). In detail, as rock strength contrast decreases, the difference in the speed of propagation between the soft and hard rock units decreases, leading to less significant changes in landscape

form and erosion rate patterns (Figure 11). Thus, in the horizontal example, with large strength contrasts as described earlier, the knickpoint that develops in the underlying hard rock propagates significantly slower than the speed of adjustment of the channels within the overlying soft rock, leading to large portions of the landscape dominated by low erosion rates (e.g. Figures 11A, 11B, and 11C). As the speed of knickpoint propagation within the underlying hard rock approaches that of the overlying soft rock, the amount of the landscape occupied by low erosion rates decreases and the rate at which the channels developed within the underlying hard rock return to equilibrium profiles is relatively quick (e.g. Figures 11D and 11E). In all models, independent of contact geometry or whether hard rocks overly soft rocks or vice versa, a decrease in the magnitude and duration of landscape disequilibrium with decreasing rock strength contrasts is clearly visible in average time series of average erosion rates (Figure 12).

Discussion

Implications for landscape evolution

Perhaps the most striking result from the modeling is the persistence of non-steady-state conditions (i.e. erosion rates not equal to uplift rates) as long as more than one unit is exposed within the landscape (Figures 2–10), and in some cases persisting even after the contact has completely eroded away (e.g. Figure 2E). In detail, the extent of the landscape within which erosion rates departed significantly from uplift rates was the greatest in models where soft rocks overlie hard rocks (Figures 2–6). By comparison, in models where hard rocks overly soft, the portion of the landscape eroding at rates substantially different than the uplift rate was primarily limited to regions near the contact (Figures 7–10). The magnitude of the departure of erosion rates from uplift rates also varies with the details of the stratigraphy, with hard over soft cases characterized by erosion rates greater than the uplift rate, where as soft over hard models have average erosion rates less than the uplift rate (Figures 2–10, 12). Contact geometry also plays a role, with increases in dip tending to increase the localization of departures from steady-state close to the contact, counter intuitively indicating that the simplest geologic settings, i.e. sub-horizontal stratigraphy, may exhibit the largest departures from steady-state, and the most complex patterns of landscape evolution, driven entirely by contrasts in rock strength (e.g. Figures 2, 12). Similarly, we observe complex landscape responses to migration of contacts, with isolated areas of depressed erosion rates leading to divide migration and drainage area capture (e.g. Figure 5A4, Movie S4, Willett *et al.*, 2014). Finally, the degree of contrast between the strength of the hard and soft rocks influences the magnitude of the deviation from steady-state denudation (Figure 12). In general, larger contrasts, or in the cases of our models, smaller K values for the harder rocks as we did not vary the strength of the soft rock, lead to larger deviations in erosion rate from the uplift rate. In considering the applicability of these results, it is important to recall that the factor of five difference in erodibility that we simulate is significantly smaller than the estimated five-orders of magnitude differences in erodibility assumed to be possible in natural landscapes (e.g. Stock and Montgomery, 1999; Sklar and Dietrich, 2001; Bursztyn *et al.*, 2015).

A related feature of the models is that elevated erosion rates, whether elevated above the uplift rate (e.g. Figure 7E) or simply elevated above the average erosion rates of the landscape

Hard over Soft Rocks - Dipping Away 35°

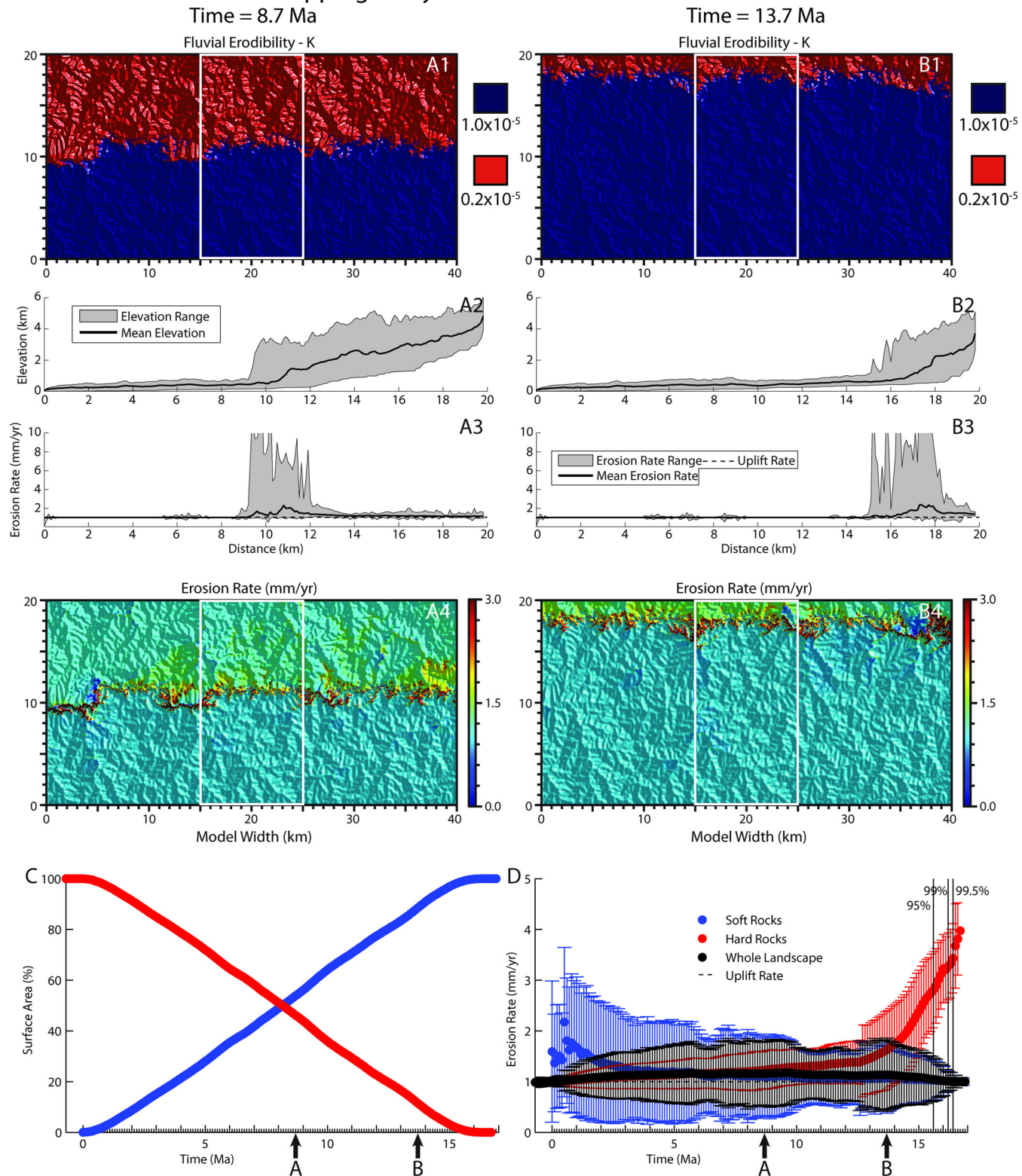


Figure 9. Selected results from two time steps (A and B) of hard over soft model with a contact dipping 35° away from the outlet, a hard rock K value of 0.2×10^{-5} yr $^{-1}$, and a soft rock K value of 1.0×10^{-5} yr $^{-1}$. Setup for this figure is the same as in Figure 7. See Supporting Information Movie S9 and Figure S10 for additional results from this model. This figure is available in colour online at wileyonlinelibrary.com/journal/espl

(e.g. Figure 2E), are not restricted to the soft rocks, as is often assumed or inferred in discussions of the influence of rock-strength on erosion rates, and specifically on rates of sediment production (e.g. Hooke, 1972; Hooke and Rohrer, 1977; Syvitski and Milliman, 2007; Portenga and Bierman, 2011). In detail, during the migration of a contact through a landscape, both the soft and hard rocks can experience periods of elevated erosion rates (Figures 2–10). Thus, while the

inherent strength of the rock controls the erodibility (i.e. the K value), the actual erosion rates of different rock types within a landscape will depend on the current landscape form and the past landscape evolution, which will be partially dictated by the geometry of the contact and the order and erodibilities of the different rock types in the stratigraphy. Thus in landscapes carved into a stratigraphic succession with variable rock erodibility landscape-mean erosion rates may well

Hard over Soft Rocks - Dipping Toward 35°

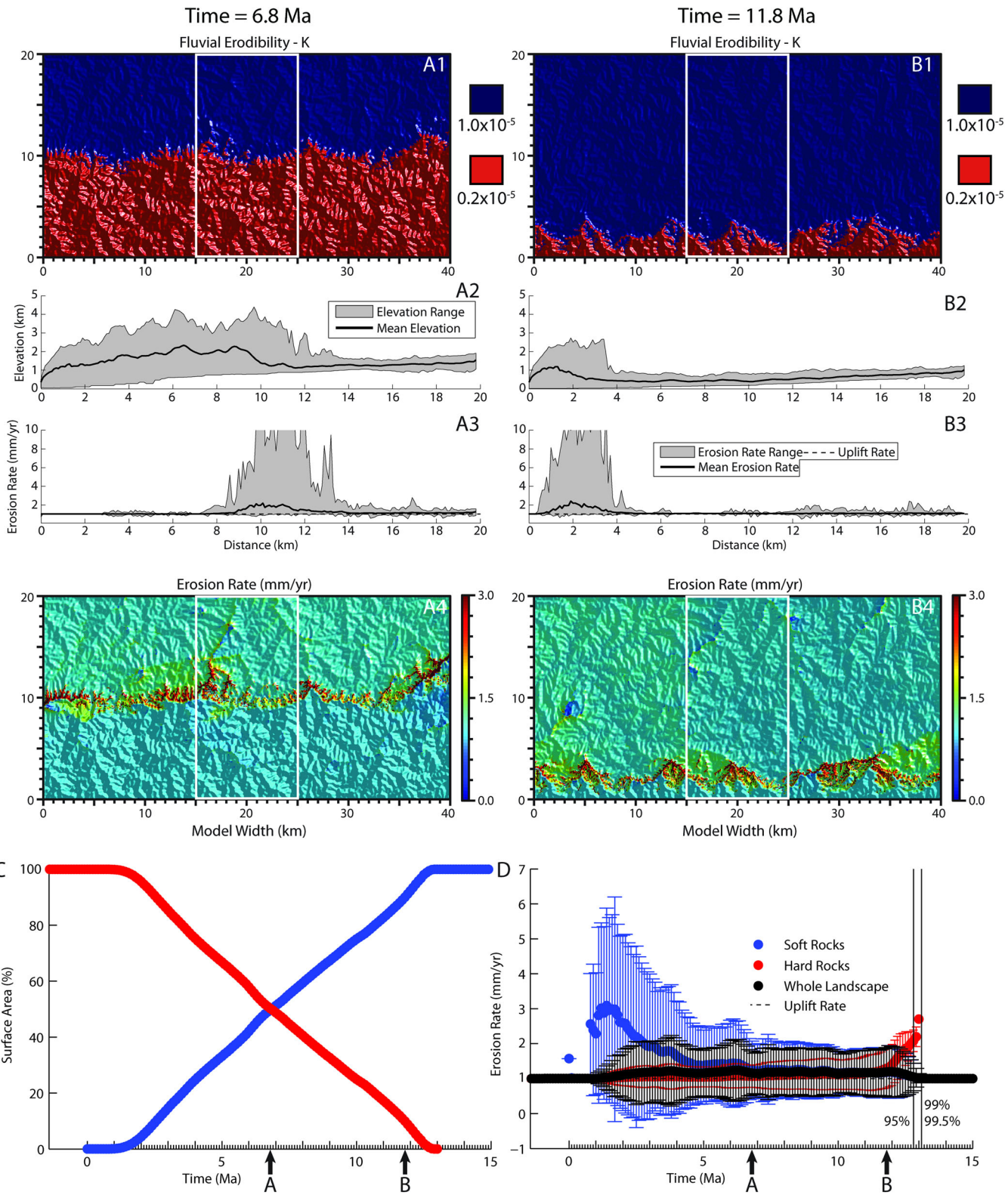


Figure 10. Selected results from two time steps (A and B) of hard over soft model with a contact dipping 35° toward the outlet, a hard rock K value of 0.2×10^{-5} yr $^{-1}$, and a soft rock K value of 1.0×10^{-5} yr $^{-1}$. Setup for this figure is the same as in Figure 7. See Supporting Information Movie S10 and Figure S11 for additional results from this model. This figure is available in colour online at wileyonlinelibrary.com/journal/espl

approach steady-state values, but erosion rates may be higher or lower than average in either the harder rocks or softer units, depending on geometry and the stage of landscape evolution (e.g. Marshall and Roering, 2014).

While our models deal with extremely simple geology (i.e. two units with a planar contact), the results are generally applicable to multi-layered stratigraphy as well. If strong contrasts in

rock strength exist between units within a landscape, unless the units are too thin to manifest at landscape scale, all the effects illustrated here will occur, only in more complex patterns, and significant spatio-temporal variability in erosion rates will persist even under steady climate and rock uplift (Figure 13, Figure S12). To confirm that more realistic, but still simple contrasts in rock strength with multiple units will still display such

Soft over Hard Rocks - Horizontal - Time = 0.4 Ma

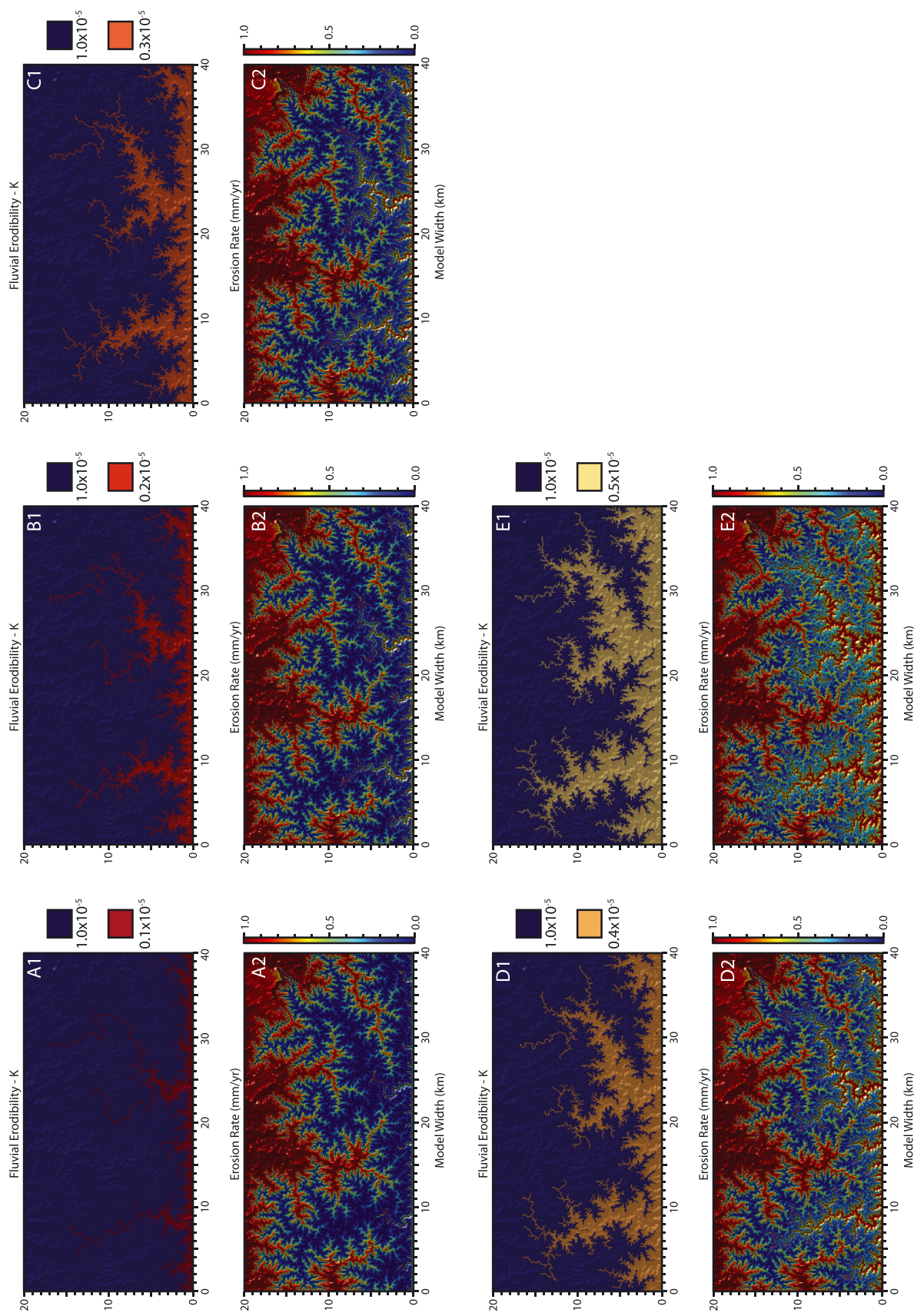


Figure 11. Selected results from the same time step of the soft over hard model with a horizontal contact and a soft rock K value of 1.0×10^{-5} yr^{-1} , but with increasing hard rock K value, i.e. decreasing strength contrast, with hard rock K values of 0.1×10^{-5} yr^{-1} (A), 0.2×10^{-5} yr^{-1} , which is identical to Figure 2A (B), 0.3×10^{-5} yr^{-1} (C), 0.4×10^{-5} yr^{-1} (D), and 0.5×10^{-5} yr^{-1} (E). Maps of the distribution of K value (top) and erosion rate (bottom) are presented for each different hard rock K value. This figure is available in colour online at wileyonlinelibrary.com/journal/espl

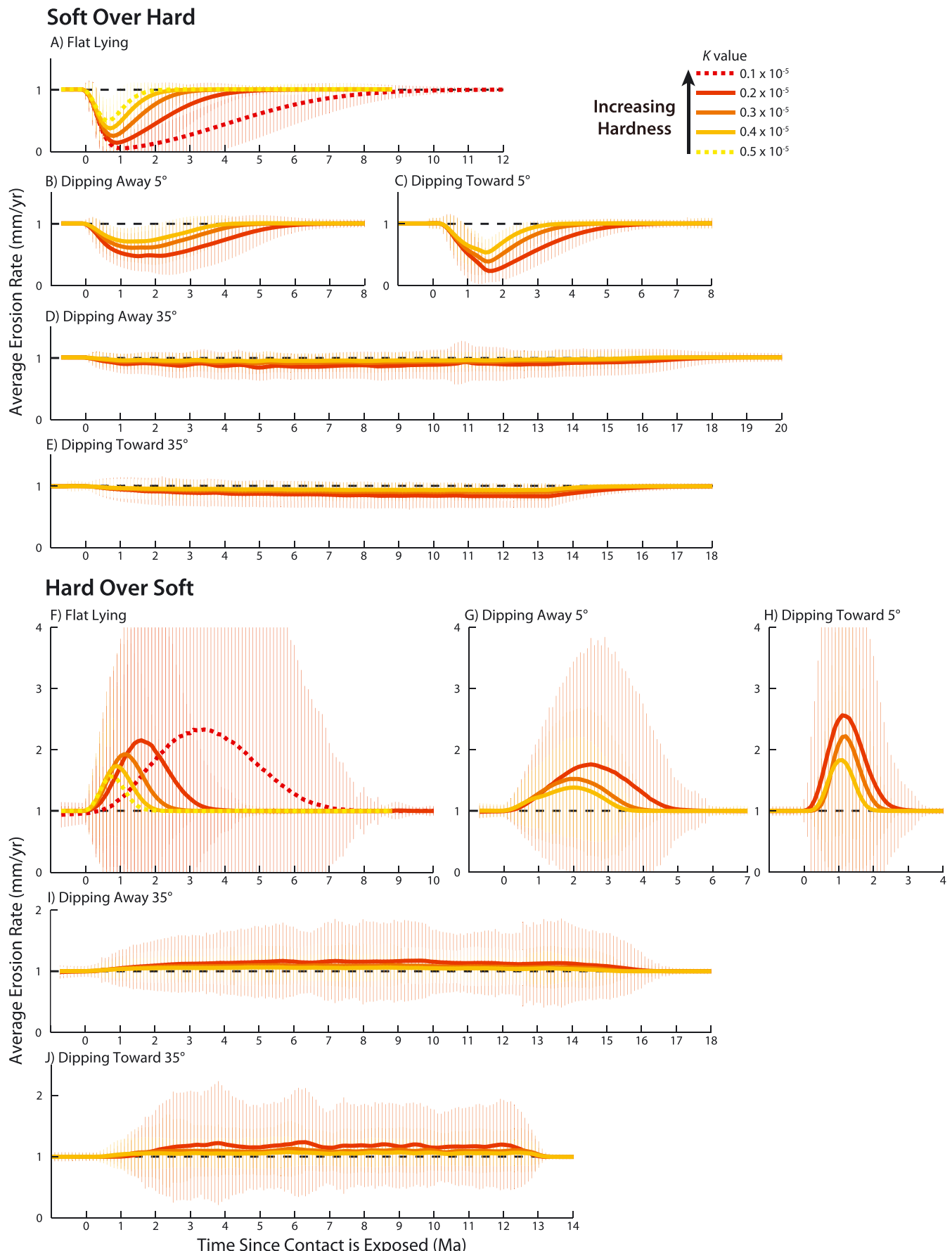


Figure 12. Average landscape erosion rates for models illustrating the effect of decreasing contrast in rock strength. Top, results from soft over hard rock models with contacts that are (A) flat lying, (B) dipping 5° away from the outlet, (C) dipping 5° toward the outlet, (D) dipping 35° away from the outlet, and (E) dipping 35° toward the outlet. Bottom, results from hard over soft rocks with contacts that are (F) flat lying, (G) dipping 5° away from the outlet, (H) dipping 5° toward the outlet, (I) dipping 35° away from the outlet, and (J) dipping 35° toward the outlet. Thick lines are the whole landscape average erosion rate; thin vertical lines are one standard deviation. Colors of lines indicate different *K* values and dashed lines indicate values of *K* only used in horizontal contact models. Soft rock *K* value is 1.0×10^{-5} yr.⁻¹. This figure is available in colour online at wileyonlinelibrary.com/journal/espl

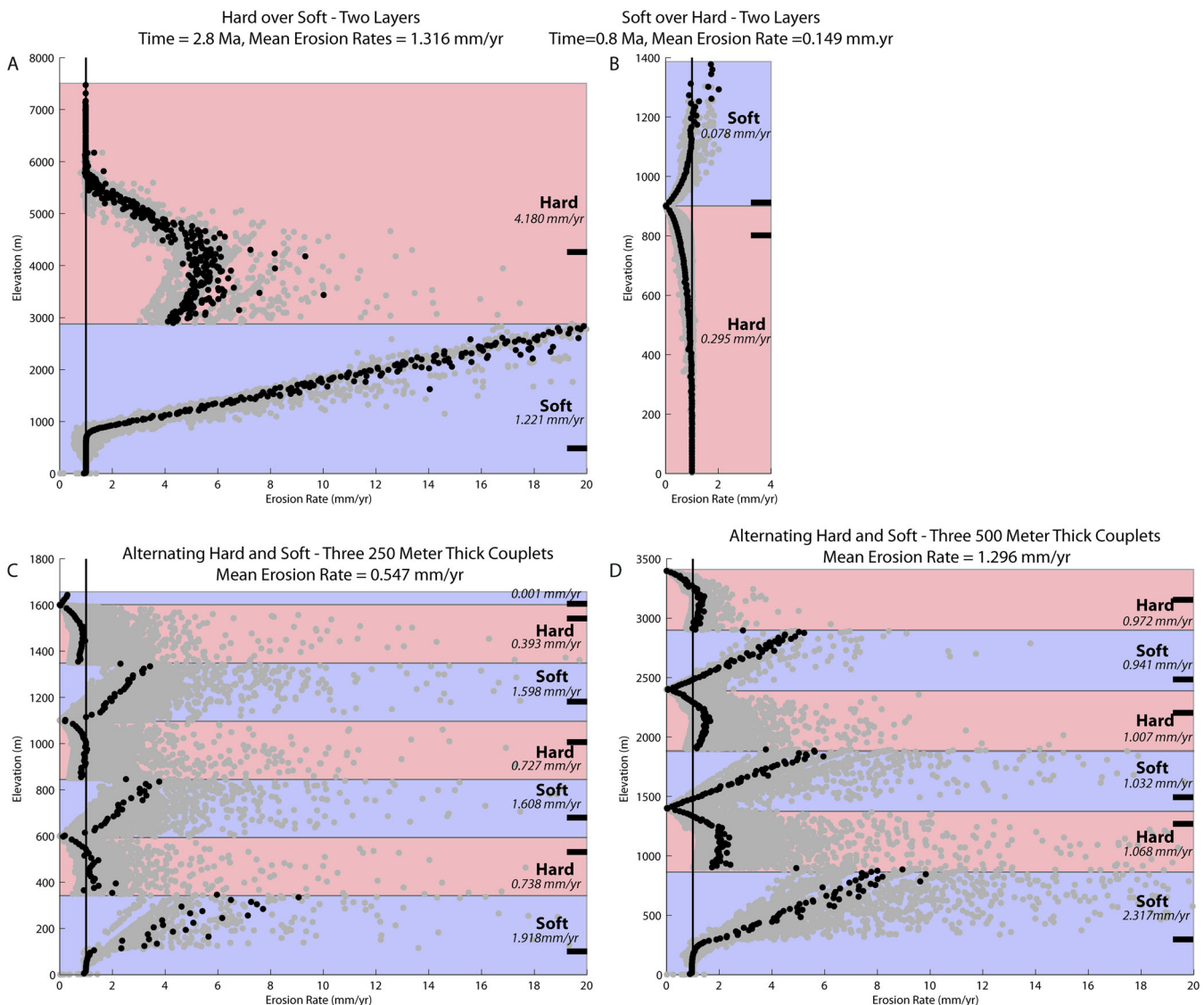


Figure 13. Erosion rates as a function of elevation from selected time steps for models with horizontal contacts and (A) two layers with hard over soft rocks, (B) two layers with soft over hard, (C) alternating hard and soft rocks in three 250 m couplets (i.e. each hard rock layer is 250 m thick and separated by a 250 m thick soft rock) with the couplets over and underlain by soft rock (see Supporting Information Figure S12 A for stratigraphic column), and (D) same as C but with 500 m unit thicknesses. Colored and labeled bands indicate hard and soft rocks and contacts between them. Vertical black line is uplift rate. Gray dots are erosion rates from all nodes within the model domain; black dots are average erosion rates over 10 m bins of elevations. Average erosion rate for the whole landscape and average erosion rate by units are reported on figure. Thick black, short horizontal lines indicate mean elevation for each unit. Notice similarity between the erosion rate patterns at contacts between hard over soft and soft over hard rocks in the alternating layers to the simple, two layer models. Reported time for two layer models is same as in other plots and is relative to time of first exposure of the contact. This figure is available in colour online at wileyonlinelibrary.com/journal/espl

departures from steady-state, we ran three models of the same dimensions and setups as the models discussed in this paper, but with three alternating layers of soft and hard rock with K values of 1.0×10^{-5} and 0.2×10^{-5} , respectively, thicknesses of 250, 500, and 1000 m, and horizontal contacts (Figure S12 A). While it is beyond the scope of this paper to discuss the detailed landscape responses observed in these models, extracting erosion rates of the different units and the landscape as a whole with time demonstrates that the variability observed in our models is not a product of their simplicity. Rather, these preliminary results suggest that erosion patterns within landscapes with alternating hard and soft rocks display the same behaviors as in two layer models, with depression of erosion rates below the uplift rate at soft over hard contacts (Figures 13B, 13C, and 13D) and erosion rates above the uplift rate at hard over soft contacts (Figure 13A, 13C, and 13D). A crucial factor in multi-layered models is the thickness of the units, with thinner units (but those still thick enough to be

manifest on the landscape scale) leading to more complicated responses as multiple units are exposed within the landscape at once (e.g. Figure 13C, Figure S12B), whereas as unit thickness increases erosion rate patterns approach a simple alternation between soft over hard rock and hard over soft rock cases as shown in our main, two layer models (Figure 13D, Figures S12C and S12D). As in the two layer models, the multi-layered landscape only reaches a denudational steady-state when a single unit is exposed throughout the landscape (Figure S12). Ultimately, determining the tradeoffs between unit thicknesses, ratios in erodibility, and the resulting degree of perturbation of a landscape represent an important direction for future work.

Applicability to natural landscapes

Our results indicate that significant departures from steady-state erosional conditions within a landscape are the most

extreme when the stratigraphy is nearly horizontally bedded and the strength contrasts between individual rock units are large. Thus, these results are the most applicable to regions meeting these criteria, namely passive margins or uplifted remnants of passive margins, e.g. the Colorado Plateau, where strong rock strength contrasts between different siliciclastic or carbonate units abound and bedding dips are gentle over large areas. In contrast, landscapes developed in more deformed rocks may have smaller departures from erosional-steady state, at least in terms of departures driven solely by rock type, for two main reasons. First, as our results highlight, increasing dip of contacts leads generally to decreases in the magnitude of departures from erosional steady-state (Figure 12), thus in regions with significantly inclined contacts, our models predict relatively modest departures from erosional steady-state. Secondly, substrate erodibility, i.e. K , is not dictated by rock type alone, but also by properties like fracture density, thus regions that have been heavily deformed by brittle processes may exhibit a more uniform K between different rock types that are similarly fractured (e.g. Molnar *et al.*, 2007; Marshall and Roering, 2014). However, it is important to realize that our results are still applicable, and thus the potential for significant departures from erosional steady state driven by contrasts in erodibility are still possible, in heavily deformed regions if the contrasts in erodibility, i.e. K , are between deformed and undeformed rocks and the boundaries between them are at a low-angle. One example of this might be the contrasts in rock strength between the brittlely deformed and fractured hanging-wall and ductilely deformed footwall within metamorphic core complexes. Additionally, at present we have modeled large, planar dipping contacts, thus it is unclear from our results whether more complicated contact geometries resultant from deformation, e.g. a series of tight folds deforming units with strength contrasts, might produce complicated landscape evolution patterns and significant departures from erosional steady-state. This represents an exciting direction for future work.

Implications for detrital records

The variability in landscape form, associated spatial patterns in erosion rates, and the time required for the contacts to migrate through the landscape combine to produce significant potential changes in the source of sediment through time. This has important implications for detrital mineral records or proxies (e.g. catchment averaged erosion rates, detrital zircon geochronology, or detrital thermochronology), which generally assume constant erosion and sediment production rates within a sampled area. Thus spatial variability in erosion rates that speed or suppress erosion within one unit will introduce a bias into detrital records, manifest as either enrichments or depletions of the detrital record with respect to particular units. If the average erosion rate within a unit is above the uplift rate, e.g. hard rocks in almost all hard over soft rock cases (Figures 7–10), or above the erosion rate of the other unit, e.g. hard rocks in the soft over hard rock with a horizontal contact case (Figure 2), then the detrital record will be enriched with respect to that unit and in these particular cases, enriched in components from the hard rock, the opposite of what might otherwise be assumed based on erodibility contrasts (e.g. Hooke, 1972; Hooke and Rohrer, 1977; Syvitski and Milliman, 2007; Portenga and Bierman, 2011). In contrast, depletion of components from a particular unit within the detrital record will occur if erosion rates within that unit are preferentially depressed below the uplift rate or below the erosion rate of the other unit. In detail, the magnitude of potential biases to detrital records will be a

product of both the variability in erosion rates within particular units and the relative proportion of that unit experiencing elevated or depressed erosion rates. This potential biasing would further exacerbate biasing from other effects, like variable concentration of the target mineral between units (e.g. Amidon *et al.*, 2005a, 2005b; Carretier *et al.*, 2015).

Our results also highlight the importance of paired topographic and geologic analysis when selecting sample sites for modern detrital record studies (e.g. catchment averaged cosmogenic erosion rates, detrital thermochronology or detrital provenance techniques). In many ways, the channel profiles or chi-z plots for model channels (Supporting Information Figures S1–S11) are not noticeably different than what is expected for transient river profiles developed in response to changes in uplift rates (e.g. Kirby and Whipple, 2012; Royden and Perron, 2013). However, unlike the adjustment to a change in uplift rate where erosion rates measured in tributaries to a main stem above and below a knickpoint should reflect the previous and new uplift rates, respectively, measured erosion rates may not reflect uplift rates if the transience is instead driven by rock strength contrasts. Based on river profile analysis alone, distinguishing between rock strength contrasts and a change in uplift rate is generally not possible, but pairing this profile analysis with detailed investigations of the geology and spatial patterns of erosion rates may be revealing. In general, if significant changes in lithology or degree of deformation coincide with significant changes in landscape and river profile form, then, inferring a change in rock strength as the causation for the changes in landscape form is warranted. It is also important to note that in general, the majority of potential variations in erosion rates with respect to uplift rates occur upstream of contacts, so for modern detrital techniques, sampling tributaries with catchment areas completely downstream of major contacts may insulate results from potential biasing. Ultimately, these results present the largest challenge for detrital mineral techniques within the stratigraphic record, where generally the form of the landscape that contributed sediment is unknown.

Limitations of our modeling approach

We believe the LithoCHILD modeling produces robust results, but it is important to consider them within the context of the simplifying assumptions embedded in the model. One important caveat is that laboratory results suggest that simple detachment limited incision models, which neglect the complicated relationships and feedbacks between amount and caliber of sediment and the magnitude of bedrock erosion, may overestimate the differences in relief predicted to develop between rocks of different erodibilities (e.g. Sklar and Dietrich, 2001) because channels may adjust bed cover, bed material grain size, and channel width in addition to channel gradient, which is the only responding variable in LithoCHILD. This is one reason why we chose to model a relatively restricted range of erodibility contrasts (i.e. at maximum a single order of magnitude as opposed to the five-orders of magnitude suggested from field studies) as we do not expect these effects to be as important in systems with more modest contrasts in strength like those we model.

Additionally, simple detachment limited models do not incorporate processes that occur at oversteepened escarpments developed beneath resistant caprocks, such as rock-mass failures in both the overlying hard and soft rock (e.g. Howard, 1995; Haviv *et al.*, 2010; Ward *et al.*, 2011). The most important likely difference between LithoCHILD with its core detachment-limited river incision assumption and models that

incorporate the role of sediment flux and variable bed cover (e.g. Whipple and Tucker, 2002; Sklar and Dietrich, 2006; Gasparini et al., 2007; Lague, 2010) is that the latter would predict blurred, or more diffuse, transitions in topographic form and erosion rate at unit contacts. Indeed, in the extreme of fully transported-limited conditions, landscapes are insensitive to local lithologic variation (i.e. insensitive to variations in K) with erosion rate, rather such conditions are only sensitive to the sediment flux and caliber from points upstream. Lithologic variation would influence sediment caliber, and the direct relation between landscape form and lithologic variation would likely not develop in a fully transport limited landscape. Landscapes spatially dominated by weak rocks but with an abundant supply of durable coarse clasts from localized sources are the most likely to fall into the transport-limited regime (e.g. Whipple and Tucker, 2002; Johnson et al., 2009; Yanites and Tucker, 2010). However, despite the prevalence of mixed alluvial-bedrock channels in nature (e.g. Howard, 1998), landscapes that exhibit pronounced lithologic control are commonplace (e.g. Ritter et al., 2011).

Conclusions

The results of our modeling study indicate that contrasts in rock strength and the orientation of contacts between different rock types induce changes in landscape form that impart significant variations in erosion rates throughout a landscape. The results further suggest that landscapes characterized by large contrasts in rock strength (but still modest in comparison to the absolute range of erodibility contrasts suggested for natural landscapes) will not reach steady-state erosion rates until only one rock unit is exposed. The perturbations in erosion rates throughout the landscapes during the passage of a contact imply that detrital records from landscapes characterized by large contrasts in rock strength may be biased and that the assumption of uniform erosion rates within many detrital techniques is problematic. The largest departures from steady-state erosional conditions, and thus the largest potential biases in detrital records, occur in landscapes with horizontal contacts and soft rocks overlying hard rocks. For dipping strata, variation in erodibility still produces significant changes in landscape form, but variations in erosion rates are more muted as the development of local base levels is not as severe. Many interesting results manifest in these simple model runs, including scenarios in which hard rock erode faster than soft rocks, the landscape as a whole erodes faster or slower than the uplift rate depending on the stratigraphy, and the direction of contact migration (i.e. does it propagate toward or away from river mouths) depends on the contact dip.

These models represent simple cases with only two units with a planar contact and dip directions parallel to the dominant direction of stream flow. Few natural landscapes present this level of simplicity, thus future work will focus on exploring whether similar (or more complicated) effects result when more complex scenarios are considered, however preliminary results suggest that the simple two-layer models may be reasonable predictors for individual contacts within more complicated stratigraphies (e.g. Figure 13). Additionally, exploring the extent to which potential biases in sediment flux observed in these models are theoretically detectable in various detrital techniques is an active line of inquiry.

Acknowledgements—The Arizona State University, School of Earth and Space Exploration (SESE) Exploration Postdoctoral Fellowship awarded to AMF supported this work. BJT developed the LithoCHILD modifications with support from Nationale Genossenschaft für die Lagerung

radioaktiver Abfälle (NAGRA), LithoCHILD code available from BJT upon request. Reviews from Dylan Ward and an anonymous reviewer along with comments from associate editor Josh Roering improved this manuscript.

References

- Ahnert F. 1970. Functional relationships between denudation, relief, and uplift in large mid-latitude drainage basins. *American Journal of Science* **268**: 243–263.
- Amidon WH, Burbank D, Gehrels GE. 2005a. Construction of detrital mineral populations: insights from mixing of U-Pb zircon ages in Himalayan rivers. *Basin Research* **17**: 463–485. DOI:10.1111/j.1365-2117.2005.00279.x.
- Amidon WH, Burbank D, Gehrels GE. 2005b. U-Pb zircon ages as a sediment mixing tracer in the Nepal Himalaya. *Earth and Planetary Science Letters* **235**: 244–260.
- Bande A, Horton BK, Ramírez JC, Mora A, Parra JL, Stockli DF. 2012. Clastic deposition, provenance, and sequence of Andean thrusting in the frontal Eastern Cordillera and Llanos foreland basin of Columbia. *Geological Society of America Bulletin* **124**: 59–76.
- Berlin MM, Anderson RS. 2007. Modeling of knickpoint retreat on the Roan Plateau, western Colorado. *Journal of Geophysical Research* **112**. DOI:10.1029/2006JF000553.F03S06
- Bhatia MR. 1985. Rare earth element geochemistry of Australian Paleozoic graywackes and mudrocks: Provenance and tectonic control. *Sedimentary Geology* **45**: 97–113.
- Bierman PR, Nichols KK. 2004. Rock to sediment – slope to sea with ^{10}Be – rates of landscape change. *Annual Review of Earth and Planetary Sciences* **32**: 215–235.
- Bursztyn N, Pederson JL, Tressler C, Mackley RD, Mitchell KJ. 2015. Rock strength along a fluvial transect of the Colorado Plateau – quantifying a fundamental control on geomorphology. *Earth and Planetary Science Letters* **429**: 90–100.
- Carrapa B. 2010. Resolving tectonic problems by dating detrital minerals. *Geology* **38**: 191–192.
- Carrapa B, DeCelles PC, Reiners PW, Gehrels GE, Sudo M. 2009. Apatite triple dating and white mica $40\text{Ar}/39\text{Ar}$ thermochronology of syntectonic detritus in the Central Andes: a multiphase tectonothermal history. *Geology* **37**: 407–410.
- Carrapa B, Strecker MR, Sobel ER. 2006. Cenozoic orogenic growth in the Central Andes: evidence from sedimentary rock provenance and apatite fission track thermochronology in the Fiambalá Basin, southernmost Puna Plateau margin (NW Argentina). *Earth and Planetary Science Letters* **247**: 82–100.
- Carretier S, Regard V, Vassallo R, Martinod J, Christophoul F, Gayer E, Audin L, Lagane C. 2015. A note on ^{10}Be -derived mean erosion rates in catchments with heterogeneous lithology: examples from the western Central Andes. *Earth Surface Processes and Landforms* **40**: 1719–1729. DOI:10.1002/esp.3748.
- Cawood PA, Hawkesworth CJ, Dhuime B. 2012. Detrital zircon record and tectonic setting. *Geology* **40**: 875–878. DOI:10.1130/G32945.1.
- Cawood PA, Nemchin AA, Freeman M, Sircombe K. 2003. Linking source and sedimentary basin: Detrital zircon record of sediment flux along a modern river system and implications for provenance studies. *Earth and Planetary Science Letters* **210**: 259–268.
- Cecil MR, Ducea MN, Reiners PW, Gehrels GE, Mulch A, Allen C, Campbell I. 2010. Provenance of Eocene river sediments from the central northern Sierra Nevada and implications for paleotopography. *Tectonics* **29**(6). DOI:10.1029/2010TC002717.
- Clarke BA, Burbank D. 2010. Bedrock fracturing threshold hillslopes, and limits to the magnitude of bedrock landslides. *Earth and Planetary Science Letters* **297**: 577–586.
- Clayton K, Shamoon N. 1998. A new approach to the relief of Great Britain II. *A classification of rocks based on relative resistance to denudation*. *Geomorphology* **25**: 155–171.
- Clayton K, Shamoon N. 1999. A new approach to the relief of Great Britain III. *Derivation of the contribution of neotectonic movements and exceptional regional denudation to the present relief*. *Geomorphology* **27**: 173–189.
- Cook KL, Whipple KX, Heimsath AM, Hanks TC. 2009. Rapid incision of the Colorado River in Glen Canyon – insights from channel

- profiles, local incision rates, and modeling of lithologic controls. *Earth Surface Processes and Landforms* **34**: 994–1010.
- Darling A, Whipple KX. 2015. Geomorphic constraints on the age of the western Grand Canyon. *Geosphere* **11**. DOI:10.1130/GES01131.1.
- DeCelles PG, Gray MB, Ridgway KD, Cole RB, Srivastava P, Pequera N, Pivnik DA. 1991. Kinematic history of a foreland uplift from Paleocene synorogenic conglomerate, Beartooth Range, Wyoming and Montana. *Geological Society of America Bulletin* **103**: 1458–1475.
- DeCelles PG, Pile HT, Coogan JC. 1993. Kinematic history of the Meade Thrust based on provenance of the Bechler Conglomerate at Red Mountain, Idaho, Sevier Thrust Belt. *Tectonics* **12**: 1436–1450.
- DeGraaf-Surpless K, Graham SA, Wooden JL, McWilliams MO. 2002. Detrital zircon provenance analysis of the Great Valley Group, California: Evolution of an arc-forearc system. *Geological Society of America Bulletin* **114**: 1564–1580.
- Dickinson WR, Suczek CA. 1979. Plate tectonics and sandstone compositions. *American Association of Petroleum Geologists Bulletin* **63**: 2164–2182.
- Duvall AR, Kirby E, Burbank DW. 2004. Tectonic and lithologic controls on bedrock channel profiles and processes in coastal California. *Journal of Geophysical Research* **109**. DOI:10.1029/2003JF000086.F03002
- Fedo C, Nesbitt HW, Young GM. 1995. Unraveling the effects of potassium metasomatism in sedimentary rocks and paleosols, with implications for paleoweathering conditions and provenance. *Geology* **23**: 921–924.
- Fedo C, Sircombe K, Rainbird RH. 2003. Detrital zircon analysis of the sedimentary record. In Zircon, Hanchar JM, Hoskin PWO (eds). *Reviews in Mineralogy and Geochemistry*: Washington, DC; 277–303.
- Garzanti E, Vezzoli G, Lombardo B, Andó S, Mauri E, Monguzzi S, Russo M. 2004. Collision-orogen provenance (Western Alps): Detrital signatures and unroofing trends. *The Journal of Geology* **112**: 143–164.
- Gasparini NM, Whipple KX, Bras RL. 2007. Predictions of steady state and transient landscape morphology using sediment-flux-dependent river incision models. *Journal of Geophysical Research* **112**. DOI:10.1029/2006JF000567.F03S09
- Gilbert GK. 1877. Geology of the Henry Mountains. Government Printing Office: Washington, DC.
- Goldrick G, Bishop P. 1995. Differentiating the roles of lithology and uplift in the steepening of bedrock river long profiles: An example from Southeastern Australia. *The Journal of Geology* **103**: 227–231.
- Goode JR, Wohl EE. 2010. Substrate controls on the longitudinal profile of bedrock channels: Implications for reach-scale roughness. *Journal of Geophysical Research* **115**. DOI:10.1029/2008JF001188.F03018
- Hack JT. 1960. Interpretation of erosional topography in humid temperate regions. *American Journal of Science* **258-A**: 80–97.
- Harkins N, Kirby E, Heimsath AM, Robinson R, Reiser U. 2007. Transient fluvial incision in the headwaters of the Yellow River, northeastern Tibet, China. *Journal of Geophysical Research* **112**. F03S04
- Hartshorn K, Hovius N, Dade WB, Slingerland RL. 2002. Climate-driven bedrock incision in an active mountain belt. *Science* **297**: 2036–2038.
- Haviv I, Enzel Y, Whipple KX, Zilberman E, Matmon A, Stone J, Fifield KL. 2010. Evolution of vertical knickpoints (waterfalls) with resistant caprock: insights from numerical modeling. *Journal of Geophysical Research* **115**. DOI:10.1029/2008JF001187.
- Hooke RL. 1972. Geomorphic evidence for Late-Wisconsin and Holocene tectonic deformation, Death Valley, California. *Geological Society of America Bulletin* **83**: 2073–2098.
- Hooke RL, Rohrer WL. 1977. Relative erodibility of source-area rock types, as determined from second order variations in alluvial-fan size. *Geological Society of America Bulletin* **88**: 1177–1182.
- Horton BK. 2005. Revised deformation history of the central Andes: Inferences from Cenozoic foredeep and intermontane basins of the Eastern Cordillera, Bolivia. *Tectonics* **24**. DOI:10.1029/2003TC001619.
- Howard AD. 1995. Simulation modeling and statistical classification of escarpment planforms. *Geomorphology* **12**: 187–214.
- Howard AD. 1998. Long profile development of bedrock channels: Interaction of weathering, mass wasting, bed erosion, and sediment transport. In *Rivers over Rock: Fluvial Processes in Bedrock Channels*, Tinkler K, Wohl EE (eds). American Geophysical Union: Washington, DC; 297–319.
- Howard AD, Kerby G. 1983. Channel changes in badlands. *Geological Society of America Bulletin* **94**: 739–752.
- Huntington KW, Hodges KV. 2006. A comparative study of detrital mineral and bedrock age-elevation methods for estimating erosion rates. *Journal of Geophysical Research* **111**. DOI:10.1029/2005JF000454.
- Jansen JD, Codilean AT, Bishop P, Hoey TB. 2010. Scale dependence of lithological control on topography: Bedrock channel geometry and catchment morphometry in Western Scotland. *The Journal of Geology* **118**: 223–246. DOI:10.1086/651273.
- Johnson JE, Whipple KX, Sklar LS, Hanks TC. 2009. Transport slopes, sediment cover, and bedrock channel incision in the Henry Mountains, Utah. *Journal of Geophysical Research* **114**. DOI:10.1029/2007JF000862.F02014
- Kirby E, Whipple KX. 2012. Expression of active tectonics in erosional landscapes. *Journal of Structural Geology* **44**: 54–75.
- Kühnli A, Pfiffner A. 2001. The relief of the Swiss Alps and adjacent areas and its relation to lithology and structure: topographic analysis from a 250-m DEM. *Geomorphology* **41**: 285–307.
- Lague D. 2010. Reduction of long-term bedrock incision efficiency by short-term alluvial cover intermittency. *Journal of Geophysical Research* **115**. DOI:10.1029/2008JF001210.F02011
- Lamb MP, Dietrich WE. 2009. The persistence of waterfalls in fractured rock. *Geological Society of America Bulletin* **121**: 1123–1134. DOI:10.1130/B26482.1.
- Lamb MP, Finnegan NJ, Scheingross JS, Sklar L. 2015. New insights into the mechanics of fluvial bedrock erosion through flume experiments and theory. *Geomorphology* **244**: 33–55.
- Leopold LB, Bull WB. 1979. Base level, aggradation, and grade. *Proceedings of the American Philosophical Society* **123**: 168–202.
- Lifton ZM, Thackray GD, Van Kirk R, Glenn NF. 2009. Influence of rock strength on the valley morphometry of Big Creek, central Idaho, USA. *Geomorphology* **111**: 173–181.
- Marshall JA, Roering JJ. 2014. Diagenetic variation in the Oregon Coast Range: Implications for rock strength, soil production, hillslope form, and landscape evolution. *Journal of Geophysical Research: Earth Surface* **119**: 1395–1417. DOI:10.1002/2013JF003004.
- Miller JR. 1990. The influence of bedrock geology on knickpoint development and channel-bed degradataion along downcutting streams in south-central Indiana. *The Journal of Geology* **99**: 591–605.
- Moglen GE, Bras RL. 1995. The effect of spatial heterogeneities on geomorphic expression in a model of basin evolution. *Water Resources Research* **31**: 2613–2623.
- Molnar P, Anderson RS, Anderson SP. 2007. Tectonics, fracturing of rock, and erosion. *Journal of Geophysical Research* **112**. DOI:10.1029/2005JF000433.
- Montgomery DR. 2001. Slope distributions, threshold hillslopes, and steady-state topography. *American Journal of Science* **301**: 432–454.
- Montgomery DR. 2004. Observations on the role of lithology in strath terrace formation and bedrock channel width. *American Journal of Science* **304**: 454–476.
- Myrow PM, Hughes NC, Goodge JW, Fanning CM, Williams IS, Peng S, Bhargava ON, Parcha SK, Pogue KR. 2010. Extraordinary transport and mixing of sediment across Himalayan central Gondwana during the Cambrian-Ordovician. *Geological Society of America Bulletin* **122**: 1660–1670.
- Oskin ME, Burbank DW, Phillips FM, Marrero SM, Bookhagen B, Selander JA. 2014. Relationship of channel steepness to channel incision rate from a tilted and progressively exposed unconformity surface. *Journal of Geophysical Research: Earth Surface* **119**. DOI:10.1002/2013JF002826.
- Pelletier JD. 2010. Numerical modeling of the late Cenozoic geomorphic evolution of Grand Canyon, Arizona. *Geological Society of America Bulletin* **122**: 565–608. DOI:10.1130/B26403.1.
- Perron JT, Royden LH. 2013. An integral approach to bedrock river profile analysis. *Earth Surface Processes and Landforms* **38**: 570–576. DOI:10.1002/esp.3302.

- Portenga EW, Bierman PR. 2011. Understanding Earth's eroding surface with ^{10}Be . *GSA Today* **21**: 4–10. DOI:10.1130/G111A.1.
- Ritter DF, Kochel RC, Miller JR. 2011. *Process Geomorphology*. Waveland Press: Long Grove, IL.
- Roddaz M, Jérôme V, Brusset S, Baby P, Héral G. 2005. Sediment provenances and drainage evolution of the Neogene Amazonian foreland basin. *Earth and Planetary Science Letters* **239**: 57–78.
- Rosenbloom N, Anderson RS. 1994. Hillslope and channel evolution in a marine terraced landscape, Santa Cruz, California. *Journal of Geophysical Research* **99**: 14013–14029.
- Royden LH, Perron JT. 2013. Solutions of the stream power equation and application to the evolution of river longitudinal profiles. *Journal of Geophysical Research* **118**: 497–518. DOI:10.1002/jgrf.20031.
- Ruhl KW, Hodges KV. 2005. The use of detrital mineral cooling ages to evaluate steady state assumptions in active orogens: an example from the central Nepalese Himalaya. *Tectonics* **24**. DOI:10.1029/2004TC001712.
- Ruiz GMH, Seward D, Winkler W. 2004. Detrital thermochronology – a new perspective on hinterland tectonics, an example from the Andean Amazon Basin, Ecuador. *Basin Research* **16**: 413–430.
- Schmidt KM, Montgomery DR. 1995. Limits to relief. *Science* **270**: 617–620.
- Schumm SA, Lichy RW. 1965. Time, space, and causality in geomorphology. *American Journal of Science* **263**: 110–119.
- Schwanghart W, Scherler D. 2014. Short Communication: TopoToolbox 2 – MATLAB based software for topographic analysis and modeling in Earth surface sciences. *Earth Surface Dynamics* **2**: 1–7. DOI:10.5194/esurf-2-1-2014.
- Sklar L, Dietrich WE. 2001. Sediment and rock strength controls on river incision into bedrock. *Geology* **29**: 1087–1090.
- Sklar L, Dietrich WE. 2006. The role of sediment in controlling steady-state bedrock channel slope: Implications of the saltation-abrasion incision model. *Geomorphology* **82**: 58–83.
- Stock GM, Ehlers TA, Farley KA. 2006. Where does sediment come from? Quantifying catchment erosion with detrital apatite (U-Th)/He thermochronometry. *Geology* **34**: 725–728.
- Stock JD, Montgomery DR. 1999. Geologic constraints on bedrock river incision using the stream power law. *Journal of Geophysical Research* **104**: 4983–4993.
- Stock JD, Montgomery DR, Collins BD, Dietrich WE, Sklar L. 2005. Field measurements of incision rates following bedrock exposure: Implications for processes controls on the long profiles of valleys cut by rivers and debris flows. *Geological Society of America Bulletin* **117**: 174–194. DOI:10.1130/B25560.1.
- Syvitski JPM, Milliman JD. 2007. Geology, geography, and humans battle for dominance over delivery of fluvial sediment to the coastal ocean. *The Journal of Geology* **115**: 1–19.
- Tooth S, McCarthy TS, Brandt D, Hancock PJ, Morris R. 2002. Geological controls on the formation of alluvial meanders and floodplain wetlands: the example of the Klip River, Eastern Free State, South Africa. *Earth Surface Processes and Landforms* **27**: 797–815.
- Tucker GE, Lancaster ST, Gasparini NM, Bras RL. 2001. The channel-hillslope integrated landscape development model (CHILD). In *Landscape Erosion and Evolution Modeling*, Harmon RS, Doe WW (eds). Springer: New York; 349–388.
- Tucker GE, Slingerland RL. 1996. Predicting sediment flux from fold and thrust belts. *Basin Research* **8**: 329–349.
- VanLaningham S, Duncan RA, Pisias NG, Graham DW. 2008. Tracking fluvial response to climate change in the Pacific Northwest: a combined provenance approach using Ar and Nd isotopic systems on fine-grained sediments. *Quaternary Science Reviews* **27**: 497–517.
- Vezzoli G, Garzanti E, Monguzzi S. 2004. Erosion in the Western Alps (Dora Baltea basin) 1. Quantifying sediment provenance. *Sedimentary Geology* **171**: 227–246.
- Ward DJ, Berlin MM, Anderson RS. 2011. Sediment dynamics below retreating cliffs. *Earth Surface Processes and Landforms* **36**: 1023–1043. DOI:10.1002/esp.2129.
- Weissel JK, Seidl MA. 1997. Influence of rock strength properties on escarpment retreat across passive continental margins. *Geology* **25**: 631–634.
- Wernicke BP. 2011. The California River and its role in carving the Grand Canyon. *Geological Society of America Bulletin* **123**: 1288–1316. DOI:10.1130/B30274.1.
- Whipple KX. 2001. Fluvial landscape response time: How plausible is steady-state denudation? *American Journal of Science* **301**: 313–325.
- Whipple KX, Hancock GS, Anderson RS. 2000. River incision into bedrock: mechanics and relative efficacy of plucking, abrasion, and cavitation. *Geology* **112**: 490–503.
- Whipple KX, Tucker GE. 1999. Dynamics of the stream-power river incision model: implications for height limits of mountain ranges, landscape response timescales, and research needs. *Journal of Geophysical Research* **104**: 17661–17674.
- Whipple KX, Tucker GE. 2002. Implications of sediment-flux-dependent river incision models for landscape evolution. *Journal of Geophysical Research* **107**. DOI:10.1029/2000JB000044.
- Whittaker AC. 2012. How do landscapes record tectonics and climate. *Lithosphere* **4**: 160–164.
- Willett SD, Brandon MT. 2002. On steady states in mountain belts. *Geology* **30**: 175–178.
- Willett SD, McCoy SW, Perron JT, Goren L, Chen C-Y. 2014. Dynamic reorganization of river basins. *Science* **343**. DOI:10.1126/science.1248765.1248765
- Willett SD, Slingerland RL, Hovius N. 2001. Uplift, shortening, and steady state topography in active mountain belts. *American Journal of Science* **301**: 455–485.
- Wobus CW, Whipple KX, Kirby E, Snyder NP, Johnson J, Spyropoulos K, Crosby BT, Sheehan D. 2006. Tectonics from topography: procedures, promise, and pitfalls. In *Tectonics, Climate, and Landscape Evolution*, Willett SD, Hovius N, Brandon MT, Fisher D (eds). The Geological Society of America: Boulder, CO; 55–74.
- Wohl EE, Greenbaum N, Schick AP, Baker VR. 1994. Controls on bedrock channel incision along Nahal Paran, Israel. *Earth Surface Processes and Landforms* **19**: 1–13.
- Yanites BJ, Tucker GE. 2010. Controls and limits on bedrock channel geometry. *Journal of Geophysical Research* **115**. DOI:10.1029/2009JF001601.F04019

Supporting Information

Additional supporting information may be found in the online version of this article at the publisher's web site.